REPORT DOCUMENTATION PAGE

Form Approved
OMB No. 074-0188

1. AGENCY USE ONLY (Leave blank)	2. REPORT DATE 08/12/2003	3. REPORT TYPE AND DATES COVERED: FINAL REPORT

4. TITLE AND SUBTITLE

Microwave Chaotic Sources

5. FUNDING NUMBERS

6. AUTHOR(S)

A. Dmitriev, G. Kssian, L. Kuzmin

7. PERFORMING ORGANIZATION NAME(S) AND ADDRESS(ES)

Institute of Radio Engineering and Electronics, Russian Academy of Sciences MOKHOVAYA ST. 11-7, MOSCOW 125009 RUSSIA

8. PERFORMING ORGANIZATION

9. SPONSORING / MONITORING AGENCY NAME(S) AND ADDRESS(ES)

US NAVAL REGIONAL CONTRACTING CENTER, DET LONDON GOVERNMENT BUILDINGS, BLOCK 2, WING 12

10. SPONSORING / MONITORING

11. SUPPLEMENTARY NOTES

LIME GROVE, RUISLIP, MIDDLESEX HA4 8BX UNITED KINGDOM

12a. DISTRIBUTION / AVAILABILITY STATEMENT

Approved for public release, distribution unlimited

20040219145

13. ABSTRACT *(Maximum 200 Words)*

The objective of the project was a search, analysis and selection of RF devices that have potential to be used to generate chaotic oscillations and that already have mathematical models that demonstrate low-dimensional chaotic behavior. The last property potentially enables to construct the symbolic description of chaotic trajectories. The performed search and analysis show that among potential candidates traveling-wave tube (TWT) and chaotic oscillator based on microtriode are more suitable for our purposes. Chosen models are investigated as for existence of low-dimensional chaotic modes. The possibility of symbolic description of a trajectory through construction of a quasi-one-dimensional map is studied for values of parameters corresponding to low-dimensional chaotic modes. It is shown how the symbolic description can be constructed both for the model of TWT and for the model of chaotic oscillator based on microtriode.

14. SUBJECT TERMS			15. NUMBER OF PAGES 42
Microwave chaotic sources, symbolic dynamics, information theory			16. PRICE CODE
17. SECURITY CLASSIFICATION OF REPORT	18. SECURITY CLASSIFICATION OF THIS PAGE	19. SECURITY CLASSIFICATION OF ABSTRACT	20. LIMITATION OF ABSTRACT

MICROWAVE CHAOTIC SOURCES

Final Technical Report

by

Team of Professor A. Dmitriev

July 2003

United States Army

EUROPEAN RESEARCH OFFICE OF THE U.S. ARMY

London, England

CONTRACT NUMBER N° 62558-02-M-6374

Kevin Linden

CONTENTS

1. INTRODUCTION

According to the contract, the goals of this work are:

- search in the literature for and selection of sources of chaotic oscillations in radio frequency band with known models and which potentially could be used for ranging and detection problems.
- study of mathematical models of chaotic sources, identification of modes of generation of low-dimensional chaos and study of modes of chaotic generation.
- analysis of a possibility of symbolic description for systems under consideration.

Symbolic description means a representation of a continuous trajectory of a chaotic generator by means of a finite alphabet. At the moment, theoretically rigorous construction of symbolic description is possible only for a limited number of discrete time systems.

There are two methods for constructing a symbolic description known from literature:

- construction of quasi-one-dimensional maps from a flow system,
- determination of a set of unstable periodic orbits (UPO) of a chaotic attractor.

Both methods imply the procedure of embedding of an observed trajectory into a multidimensional (preferably, three-dimensional) phase space. Then a one-dimensional-one-dimensional map is constructed or a topology of the attractor by means of UPO is determined. With a successful embedding and determining of a UPO set, the known structure of the attractor facilitates determining the size of an alphabet necessary for symbolic encoding of the trajectory. Finally, UPO set enables to determine a generating partition.

This is why systems with low-dimensional chaos are considered in the literature in detail. For such systems it is possible to construct quasi-one-dimensional succession sequence, which determines generating partition and enables to solve some other problems concerning the structure of attractor. In this paper attention is paid to construction of quasi-one-dimensional maps, which might define a generating partition.

Such a sequence could facilitate comparison of signals, decision about identity of signals (fellow/stranger), synchronization of two chaotic sources. In some cases symbolic description could facilitate synchronization in the presence of additive noise or distortion of signal in a channel.

In section 2 a review is given of five models of microwave chaotic generators: klystron generator with delay, generator based on traveling-wave tube, based on backward-wave tube, Pierce diode and microtriode. Two models have been selected for further investigation: generator based on traveling-wave tube and generator based on microtriode.

Section 3 describes features of such models, their characteristics and numerical methods used for studying these models.

Existence of low-dimensional chaotic modes in selected models of generators is shown in section 4.

The description of trajectories of models of generators, selected in section 2, by means of binary symbolic sequences, is investigated in section 5.

For the system based on m. triode the symbolic description is con. cted and properties of obtained symbolic sequences are studied. Methods for constructing symbolic binary sequences closely connected with initial chaotic trajectory are indicated and properties of such sequences are considered for the system based on traveling-wave tube.

2. REVIEW OF GENERATORS

In this section a review is given of models of generators of chaotic oscillations in microwave range, presented in the literature. Best-studied and relatively simple mathematical models of generators, which have been shown to have chaotic modes are included in this review. This section includes neither detailed description of physical organization of devices nor principles of operation. More detailed material can be found in literature, cited in the body of this section.

All results of numerical or physical experiments cited in the text of this section are taken from the cited literature.

2.1 Klystron generator

The scheme of klystron generator with delayed feedback is presented in Fig. 1. Electron beam (shown with arrows) is velocity-modulated in the first resonator. Energy is taken off the beam in the second resonator. Input and output resonators are connected with the delayed feedback line. The input resonator is excited by the signal of output resonator coming from feedback line, which is characterized by modulation depth m and delay time δt. Output resonator is excited by the current of the electron beam. If voltages at cavity gaps of input and output resonators are represented as $V_{1,2}(t) = \mathrm{Re}(A_{1,2}(t)\exp(i\omega_0 t))$, the equations for excitation of resonators become [1]:

$$\frac{dA_1}{dt} + \frac{\omega_0}{2Q_1} A_1 = \frac{m\omega_0}{2Q_1} A_2(t-\delta t)\exp(-i\omega_0 \delta t), \quad (1a)$$

$$\frac{dA_2}{dt} + \frac{\omega_0}{2Q_2} A_1 = \omega_0 K I_1(l,t)\exp(-i\omega_0 l/v_0), \quad (1b)$$

where l - is the distance between the resonators, K - wave resistance of output resonator, Q_1, Q_2 - are loaded quality factors and

$$I_1(l,t) = -2iI_0 J_1(|A_1(t-l/v_0)|\theta_0/2V_0)\exp(i\varphi(t-l/v_0)) \quad (2)$$

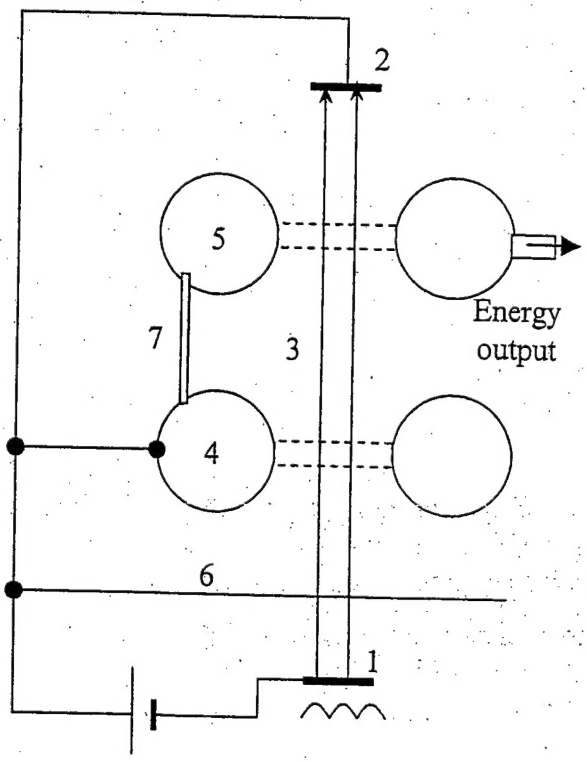

Fig. 1. Scheme of klystron generator with delay: 1 – cathode, 2 – collector, 3 – electron beam, 4,5 – input and output resonators, 6 – accelerating electrode, 7 – feedback.

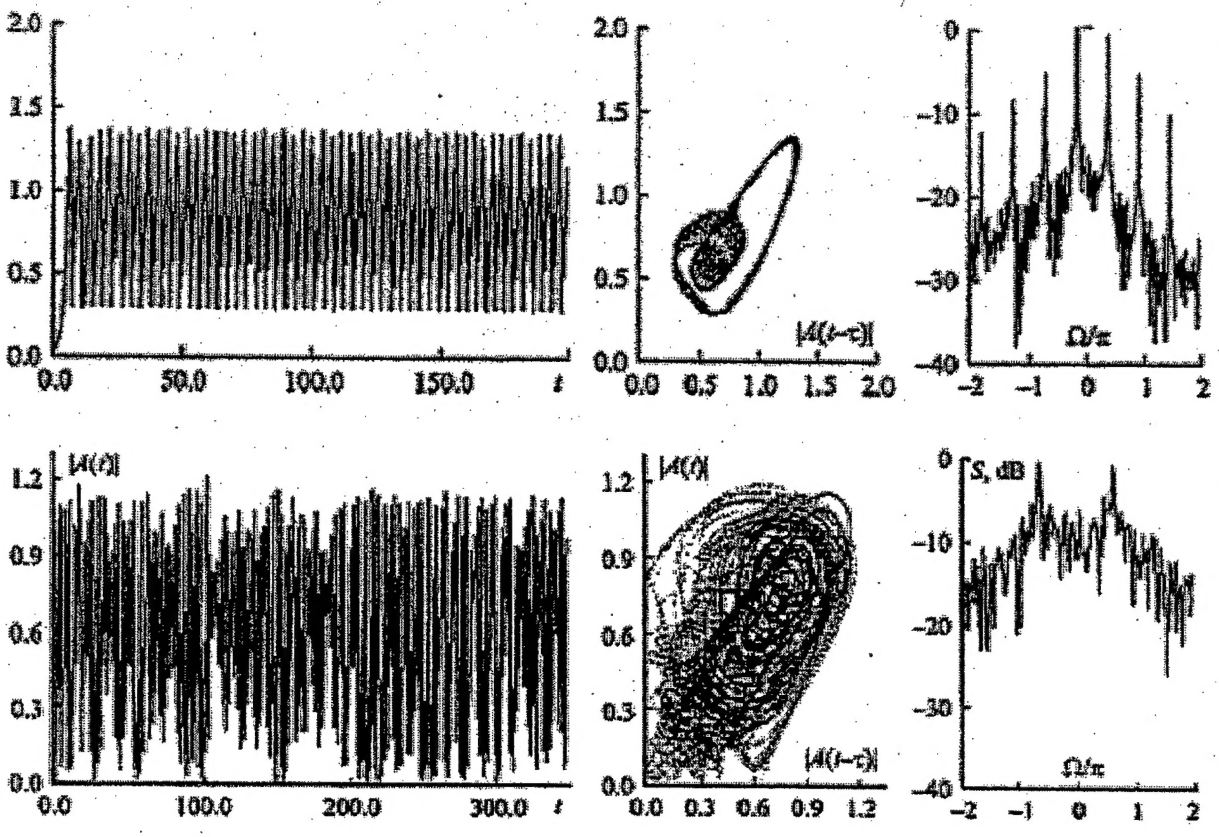

Fig 2. Waveforms, phase portrait and power spectra density for two modes of klystron generator.

is the first harmonic of the current (second resonator is usually a part of a high-Q empty resonator, so only the first harmonic of the current exciting the second resonator is considered).

J_1 is Bessel function of first order, $\varphi = Arg(A_1)$, $\theta_0 = \omega_0 l / v_0$ - is undisturbed transit angle (phase incursion).

With dimensionless amplitudes of oscillations

$$F_1(\tau) = A_1(\tau)\theta_0 / 2V_0 \tag{3a}$$

$$F_2(\tau) = \frac{mA_2(\tau - \omega_0 \delta t / \psi)\theta_0}{2V_0} \exp(-i\omega_0 \delta t), \tag{3b}$$

where $\tau = \omega_0 t / \psi$ and $\psi = \omega_0(\delta t + l / v_0)$, then

$$\begin{cases} \dfrac{dF_1}{d\tau} + \gamma_1 F_1 = \gamma_1 F_2 \\ \dfrac{dF_2}{d\tau} + \gamma_2 F_2 = 2\alpha J_1(|F_1(\tau - 1)|) \dfrac{F_1(\tau - 1)}{|F_1(\tau - 1)|} \end{cases} \tag{4}$$

where $\gamma_{1,2} = \psi / 2Q_{1,2}$ - are damping parameters, $\alpha = m\varepsilon\psi\theta_0 \exp[-i(\psi + \pi/2)]$, $\varepsilon = KI_0 / 2V_0$ - are amplification parameters.

In case of low–Q of input resonator ($\gamma_1 >> 1$) the system is reduced to a first-order equation:

$$\frac{dF}{d\tau}+\gamma_2 F = 2\alpha J_1(|F(\tau-1)|)\frac{F(\tau-1)}{|F(\tau-1)|} \qquad (5)$$

Numerical simulation was carried out for the following values of the system parameters. Length of the feedback line is 8 m, signal moves with velocity of light, distance between resonators $l = 10$ cm, fundamental frequency of resonators is $f_0 = 3$ GHz, loaded quality factors $Q_{1,2} = 300$, wave resistance $K = 100$ Ohm, accelerating voltage $V_0 = 2500$ V, current $I_0 = 50$ mA.

Values of dimensionless parameters are $\psi + \pi/2 \approx 180\pi$, $\theta_0 \approx 20\pi$, $\gamma_{1,2} \approx 1$, $\varepsilon \approx 10^{-3}$.

The work [1] includes results of numerical and physical experiments (integration by Runge-Kutta method of the fourth order) (see Fig.2). Numerical experiment demonstrates transition to chaos through series of period doubling bifurcations. The experiment corroborates also the presence of a chaotic mode. But since the experiment was carried out with five-resonator klystron, agreement with numerical experiment is only qualitative.

The results of numerical experiment are presented in greater detail in [2].

2.2. *Traveling-wave tube (TWT)*

Scheme of generator with delayed feedback based on traveling-wave tube is depicted in Fig.3.

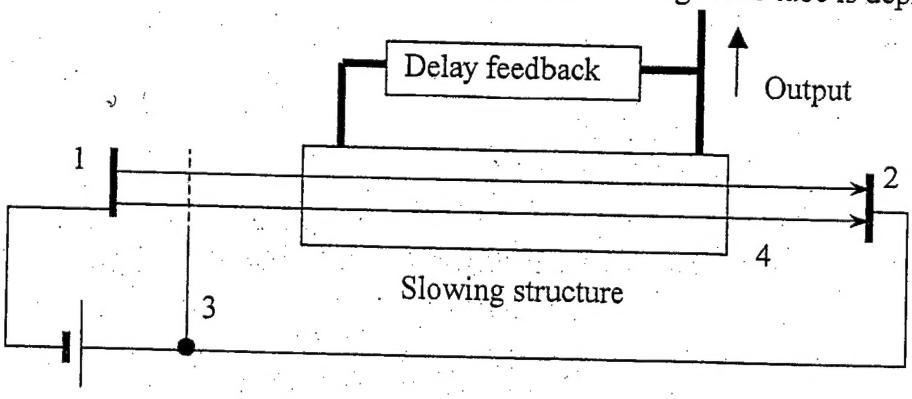

Fig. 3. Scheme of TWT-generator: 1 – cathode, 2 – anode, 3 – accelerating grid, 4 – electron beam

Advantage of TWT as compared to klystrons is amplification in a broad frequency band.

Results of experiments on searching for chaotic modes in a TWT-generator are described, e.g., in [3,4].

First, generator was considered in a general form [5,6], depicted in Fig. 4, where F – is a nonlinear amplifier, T – is a delay and Φ – is a filter.

The equation for oscillations of such generator is a functional equation:

$$X(t) = \Phi F(X(t-T)), \qquad (6)$$

where $\hat{\Phi}s(t) = \int_{-\infty}^{t} s(\tau)g(t-\tau)d\tau$, and $g(\tau)$ - is an impulse response characteristics of the filter.

For narrow-band filter and for $T = 0$ this equation corresponds to reduced differential equation

$$X' + \varepsilon X = \varepsilon F(X) \qquad (7)$$

or, in the presence of delay

$$X' + \varepsilon X = \varepsilon F[X(t-T)], \qquad (8)$$

where $\varepsilon << 1$.

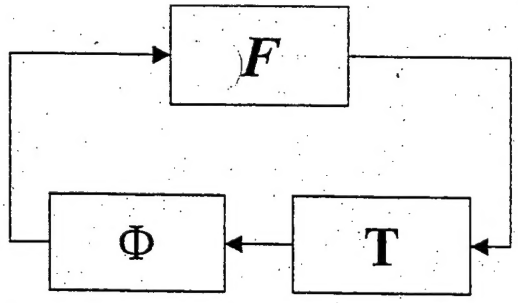

Fig. 4. Block-scheme of TWT generator

This equation is studied with cubic nonlinearity $F = \gamma_0 X(1-X^2)$ or with nonlinearity of the type $F(X) = \alpha X \exp(-(X-\beta)^2)$, which, according to [5], describes the nonlinearity of TWT in the best way.

The results of numerical simulation of the system are described in [3]. Simulation was carried out under the assumption that the field at the input area of TWT is defined, phase wave velocity is constant and is independent of signal frequency. For the input area of tube an approximation of specified current is used. Since the input signal fades completely in the local absorbent and the output signal is week and does not influence beam, the effect of volume charge is neglected.

2.3. System based of backward-wave tube (carcinotron)

Traveling-wave tube is a broadband amplifier, but it can operate as a generator only in a relatively narrow frequency band. As a broadband generator, backward-wave tube is usually used. Its scheme is depicted in Fig. 5. In such generator amplification is provided by interaction of backward wave with electron beam, which is used to transfer oscillation energy from the input of decelerating system to the output, where backward wave occurs. Thus electron beam is used simultaneously as feedback regulated by phase (to change the accelerating voltage), which provides tuning of generation frequency in a broad frequency range.

Dynamics based on backward-wave tube is described in [7], where there are also references to earlier works.

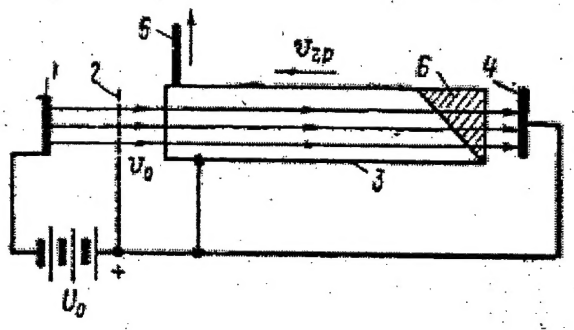

Fig. 5 Scheme of generator based on backward-wave tube: 1 – cathode, 2 – accelerating electrode, 3 – periodic decelerating system, 4 – collector, 5 – energy output, 6 – matched load

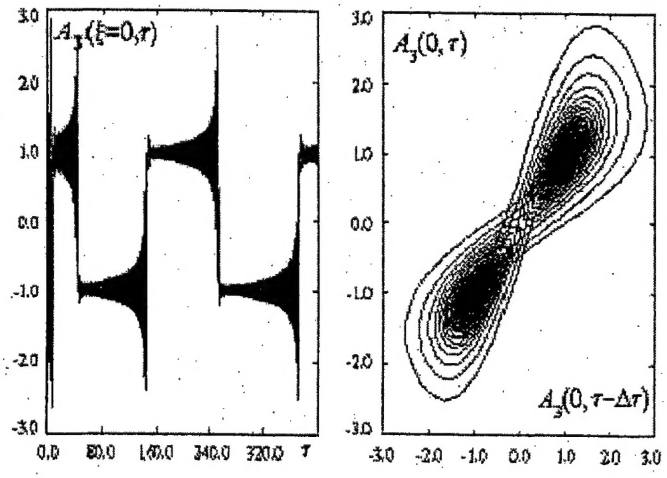

Fig. 6. Waveform and phase portrait of generator based on backward-wave tube.

It is shown that generator b. } on backward-wave tube could be des)ed by equation

$$\frac{\partial A_1}{\partial \tau}+\frac{\partial A_1}{\partial \xi}=\alpha A_2 A_3^*,$$

$$(1+u)\frac{\partial A_2}{\partial \tau}+\frac{\partial A_2}{\partial \xi}=-\alpha A_1 A_3, \qquad (9)$$

$$\frac{\partial A_3}{\partial \tau}-\frac{\partial A_3}{\partial \xi}=\alpha A_2 A_1^*.$$

Numerical simulation demonstrates considerable similarity with finite-dimensional Lorenz system (Fig. 6).

2.4. Pierce diode

Pierce diode consists of two parallel infinitely wide equipotential grids, penetrated by monoenergetic electron flow. Charge density and flow velocity at the input of the system are fixed. Space between grids are filled uniformly with motionless ions.

Control parameter is Pierce parameter $\alpha=\omega_p L/v_0$, where $\omega_p=\sqrt{e\rho/\varepsilon m}$ - is plasma frequency, ρ_0 - is charge density in the flow at the input , v_0 - flow velocity at the input, L - the distance between grids.

Pierce has shown in 1944 that uniform motion of the flow with velocity $v(x)=v_0$ becomes unstable at $\alpha>\pi$. Fluctuations of charge density in the flow lead to redistribution of charges in external circuit, connecting the grids, and to the appearance of induced charge on the bounding grids. As a result, potential at the grids remains constant, and uniform field of these charges strongly perturbs the flow. For $\alpha>\pi$ this perturbation leads to growth of fluctuations of charge density. Perturbation evolves until a virtual cathode appears in the system – a region with potential of volume charge close to cathode potential. The virtual cathode reflects part of input electron flow to input grid.

According to [8], Pierce diode could be used to obtain super-power microwave radiation. Numerical simulation is based on "particle in a cell" method. Electron beam is represented as a body of big particles (in one-dimension case – charged sheets), injected in equal time intervals with constant velocity into the interaction space. For every sheet an equation is solved:

$$\frac{d^2x_i}{dt^2}=-E(x_i) \qquad (10)$$

To calculate field strength and field potential of volume charge and charge density a uniform space grid with step Δx is introduced. Field potential of volume charge in electrostatic approximation is defined by Poisson equation:

$$\frac{\partial^2\varphi}{\partial x^2}=\alpha^2(\rho-1) \qquad (11)$$

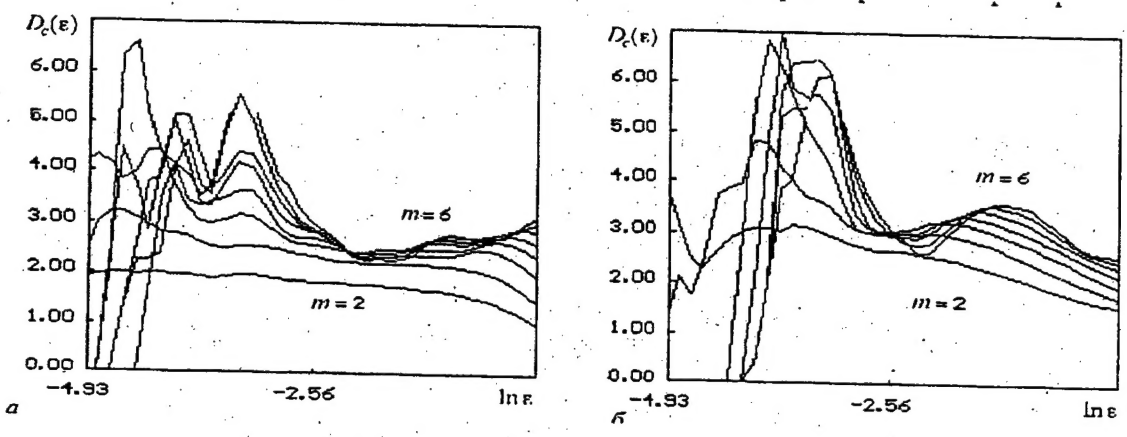

Fig. 7. Dependence of dimension D on observation scale for different dimensions of embedding space for two modes of non-regular oscillations.

To calculate charge density a procedure of linear weighting of particles on space grid is used. Field strength is calculated by differentiation of obtained values of potential. The number of grid cells is 128, and the number of particles per cell in unperturbed state is 4.

Analysis of oscillations was carried out by means of observation of time realizations of field of volume charge E at the output of the system and corresponding power spectra. Existence of chaotic modes is shown; dimension of attractor is estimated (see Fig.7).

2.5 Oscillator based on vacuum microtriode.

Study of chaotic dynamics of vacuum microtriode is described in [9]. It is shown that active microtriode oscillator can generate chaotic oscillations in microwave band.

Active oscillator could be constructed by introduction of a feedback into the scheme of microtriode amplifier in a manner similar to usual tube generator. However, due to the absence of saturation of nonlinear characteristics, self-oscillations in such generator would increase infinitely, leading to destruction of cathode. It is necessary to introduce passive element with nonlinear characteristics into feedback loop to compensate the signal growth.

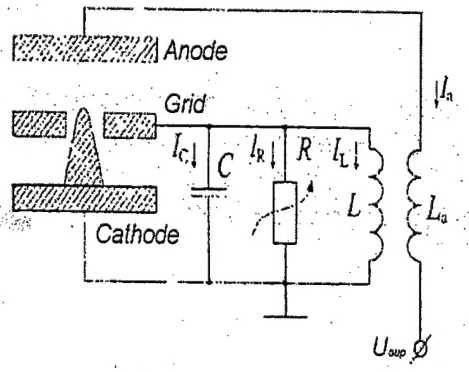

Fig. 8. Scheme of generator based on vacuum microtriode with inductive feedback and nonlinear dissipative element in the grid circuit.

Scheme of proposed generator (see Fig.8) contains a vacuum microtriode with nonlinear oscillation circuit (nonlinearity is given by resistor), included in a grid circuit, and an inductive feedback.

Anode current depends on voltage at the grid according to Fauler-Nordheim's law of autoelectronic emission:

$$I_a = AF^2(aU+b)^2 \exp[-B\Phi^{3/2}/(F(fU+b)], \qquad (12)$$

where I_a - anode current, U - grid voltage, A, B - almost constant parameters, Φ - work function, F - field amplification, a, b - geometric constants.

Nonlinear dissipation is given by nonlinear resistor, with characteristic

$$I = I_0[\exp(U/U_0) - 1] \tag{13}$$

The generator equation in dimensionless variables for non-autonomous mode is given by

$$\frac{d^2x}{d\tau^2} + (g_0 e^{k\alpha} - \mu(2x + 2\sigma + 1)e^{-(x+\sigma)^{-1}})\frac{dx}{dt} + x = V\sin(p\tau) \tag{14}$$

Existence of chaotic modes is demonstrated by physical an experiment and numerical simulation. Spectra and phase portraits are presented in [9]. Results similar to those of [9] are presented in the following sections.

2.6. Models selected for investigation

Among five models described above, capable of generating chaotic signals in microwave band, we have selected two: generator based on microtriode and generator based on traveling-wave tube.

We have preferred models that are studied to some extent and at the same time have models that do not require enormous computational resources for simulation of their dynamics.

As a result, we selected a model based on microtriode, which is described by non-autonomous ordinary differential equation of second order. This model is of interest also because generator based on microtriode is the only generator of chaotic signal in microwave region with finite dimensional model discovered in literature. All other above models are described either by differential equations with delay or by partial differential equations, i.e. by systems with infinite number of degrees of freedom.

The complexity of such system is that it is stiff and requires care in numerical simulation. Different integration methods were used for numerical simulations and chaotic modes have been obtained which are in good agreement with those described in [9]. The calculation of a trajectory could be carried out by Runge-Kutta method of 4-5 order with variable step, if constraints are imposed on maximum size of integration step.

Among models presented in this review, two are described by differential equations with delay. These are the model of klystron generator and TWT-model. For further investigation we have taken the system based on TWT, because equation (8) is simpler than system (4).

In case of necessity, developed methods for analysis of TWT-generator can be employed to analyze of the dynamics of klystron generator with delay.

Equation with delay (8), for TWT-system, has infinite number degrees of freedom, and this fact substantially complicates investigation of this system. First, chaotic modes of high dimension might exist in such system, and, as one will see from the results described below, this narrows the region of parameters useful to us. Second, calculation of equation (8) gives one scalar component, so to study chaotic modes it is necessary to reconstruct a phase space. Reconstruction algorithm is described in the next section.

3. ALGORITHMS

The aim of this section is to describe algorithms used for identification of low-dimensional chaotic modes.

By investigation of the syste based on microtriode and described by uation (14) we do not face a problem of separating the regions of high-dimensional and low-dimensional chaos. Only simple chaotic modes are possible in the system. The single aim of estimating of dimension or the major Lyapunov exponent is to give evidence that the modes are chaotic.

With TWT-system the situation is much more complicated. This system has chaotic modes of high dimension and isolation of "relatively simple" modes of low dimension is important. As was already noted, calculation of equation (8) gives the only scalar variable, so, preliminary reconstruction of a phase space and embedding of realization into this phase space is necessary (embedding algorithm is described below).

The first problem here is that embedding space dimension for calculated signal is unknown. To estimate this dimension — the embedding space dimension — the Karhunen-Loeve method could be used.

After estimation of embedding space dimension it is possible to reconstruct the phase portrait and to estimate attractor dimension using correlation integral and to calculate Lyapunov exponents.

To sum up, in this work we

1. Estimate embedding space dimension by the method of Karhunen-Loeve.
2. Estimate attractor dimension and embedding space dimension by means of correlation integral.
3. Estimate Lyapunov dimension by Lyapunov exponents.

To illustrate the methods described and verify the algorithms employed we cite the results for Rossler system

$$\begin{aligned} \dot{x} &= -y - z \\ \dot{y} &= x + ay \\ \dot{z} &= b + (x - c)z \end{aligned} \qquad (15)$$

with parameters $a = 0.15$, $b = 0.2$, $c = 10$ corresponding to simple chaotic mode. Under other values of parameters Rossler system can demonstrate much more complicated dynamics [11].

3.1. Estimation of embedding space dimension by Karhunen-Loeve method.

To construct embedding space it is necessary to get several coordinates in a multidimensional embedding phase space from one observed coordinate $x(t)$.

There are several methods for this. For instance, initial signal and its derivatives are considered as coordinates:

$$\left(x(t), \dot{x}(t), \ddot{x}(t)...\right), \qquad (16)$$

or time-delayed values of a single coordinate (Takens method of delay embedding).

$$(x(t), x(t-\tau), x(t-2\tau)) \qquad (17)$$

Review of methods for phase space reconstruction by one coordinate can be found in [12].

We use the method of (y embedding. Its idea was proposed . 13] and mathematical justification was given in [14]. The idea of justification is that subject to some conditions, topological equivalence is shown, between the initial attractor of the system and attractor reconstructed by one observed coordinate.

To determine embedding space dimension, let us consider n values of variable $X_1 = (x_1 \ldots x_n)' = (x_{t0}, x_{t0+\tau} \ldots x_{t0+\tau(n-1)})'$, taken successively in time interval τ, as a vector in n-dimensional phase space. Similarly, $X_2 = (x_2 \ldots x_{n+1})' = (x_{t0+\tau}, x_{t0+2\tau} \ldots x_{t0+n\tau})'$

Theoretically, any value of delay time τ is acceptable. Practically, too big or too small values of delay time τ complicate analysis of reconstructed attractor. The issue of optimal delay time have been discussed intensively in the literature. Optimal delay time could be taken as the first zero of autocorrelation function for observed realization, as the first minimum of mutual information function, etc. Review of possible methods is presented in [15].

In this work we define delay time as the first zero of autocorrelation function of the process. Obtained sampling proves to be in accordance with simple rule of "3-5 samples per period", cited in [16].

We also check our results on stability relative to sampling interval τ.

Thus, consider a method for estimation of embedding space dimension, described in [17], and also known in the theory of image processing as algorithm of Karhunen-Loeve [18]. According to this method, it is necessary to construct a sequence of vectors by Takens method from $N = N_T - n + 1$ points x_i, where N_T - time series length, n - phase space dimension, which is at first taken rather big, certainly bigger than expected embedding space dimension (say, 15 or 20). Then a matrix of trajectory is constructed:

$$\Sigma = N^{-1/2} \begin{bmatrix} X_1' \\ X_2' \\ \vdots \\ X_N' \end{bmatrix} \qquad (18)$$

Columns of this matrix are projections of phase trajectory on axes of n-dimensional phase space. The number of linearly independent projections, i.e., rank of matrix Σ, determines the number of coordinates required for unique description of the system state. Rank of matrix Σ equals to the number of non-zero eigenvalues of matrix $\Theta = \Sigma\Sigma'$.

Practically, due to presence of noise or due to the fact that the system is only approximately finite-dimensional, eigenvalues of matrix Θ will not go to zero, but will decrease with the eigenvalue index (and for white noise they will decrease very slowly). Thus, it is necessary to determine some threshold value and to account only for eigenvalues of covariance matrix Θ which are bigger than the threshold value.

An example of determining the dimension for Rossler attractor is depicted in Fig. 9a. Dimension is estimated by the break on the of plot covariance matrix eigenvalues. For this plot it is 2-3.

After selecting space dimension, it is possible to choose new basis from basis vectors, corresponding to "nonzero" eigenvalues. Geometrically, it means such a rotation of axes of n-dimensional phase space when phase trajectory would have nonzero projections only on $m < n$ axes.

Advantages of this meth are small requirements for computati resources and noise resistance. It is shown in [19] that successive application of this algorithm enables to get a signal substantially cleared from noise.

Besides, it is shown in [20] that development of methods based on decomposition on eigenvectors of covariance matrix enables to get estimates of attractor dimension that are operating in a broader region of sampling time τ than method based on estimation of correlation integral, described below.

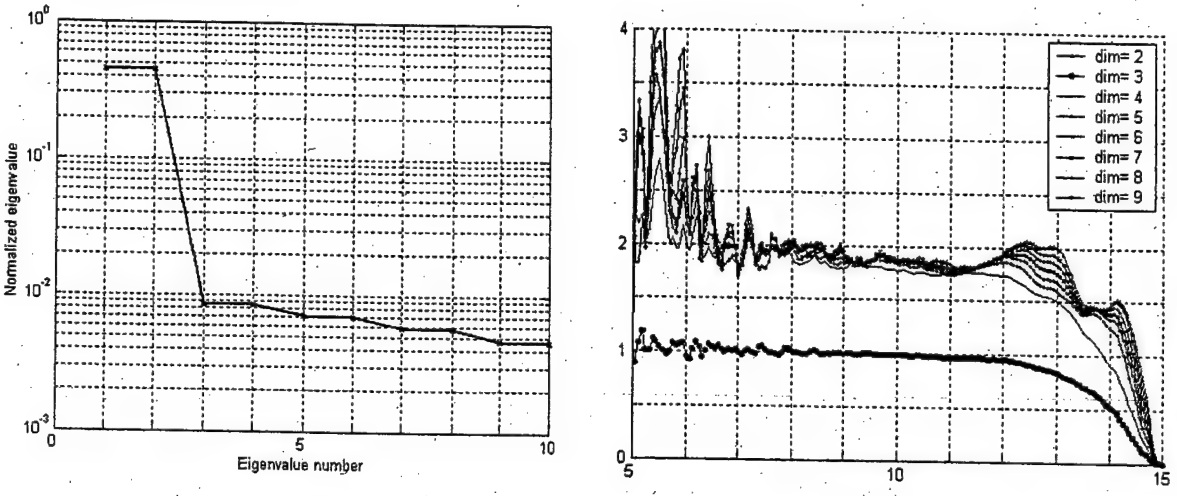

(a) (b)

Fig. 9. Results of estimation of embedding space dimension (a) and calculation of correlation dimension (b) for Rossler system (15).

3.2. Estimation of embedding space dimension by correlation integral

The second method for calculation of attractor dimension and estimation of embedding space dimension is the method of correlation integral [21].

The idea of the method is the following. The number of points in the neighborhood of radius ε grows with ε as ε^d in a space of dimension d.

To calculate dimensions, in a manner similar to that described above, n-dimensional vectors are taken from one-dimensional time series by Takens method and for sufficiently large set of vectors (more than several thousands), a number of vectors in the ε-neighborhood of some arbitrarily taken vector is calculated. An estimate d of attractor dimension is derived from obtained dependence of the number of vectors in ε-neighborhood on ε.

Practically, correlation dimension is calculated for different embedding space dimensions n. Starting from certain n, calculated attractor dimension does not change (saturates). This value of n, when saturation begins, could be considered as estimate of embedding space dimension.

Result of dimension calculation for Rossler attractor is given in Fig. 9b. Horizontal axis features different space scales (different ε). Vertical axis represents calculated attractor di-

mension. At very large or small ε error of calculation become too large. Estimation of attractor dimension is taken at "average" ε, where the curve is almost constant.

As can be seen in Fig. 9b, Rossler attractor dimension is slightly higher than two. As can be also seen, saturation takes place already at $n=3$ (which is in accordance with the fact that Rossler attractor lies in three-dimensions space).

3.3. Calculation of Lyapunov exponents and Lyapunov dimension

Lyapunov dimension is defined by

$$d_L = k + \frac{\lambda_1 + \lambda_2 + ... + \lambda_k}{|\lambda_{k+1}|}, \qquad (19)$$

where λ_i - Lyapunov exponents of the system (in decreasing order) k - maximum value subject to $\lambda_1 + \lambda_2 + ...\lambda_k > 0$.

An assumption is made in [22], supported by numerical evidence, that for "normal" attractors Lyapunov dimension equals dimension calculated by correlation integral.

For the system based on microtriode one exponent is positive and one is negative for chaotic modes. According to formula (19) this corresponds to attractor dimension being between two and three.

Thus, for this system it is sufficient to calculate only the major Lyapunov exponent. It can be calculated by standard means, i.e., by introduction of small perturbations and calculation of average rate of growth of these perturbations.

For the TWT-system, which is infinite-dimensional, such a method is inapplicable.

Algorithm of calculation of major Lyapunov exponent [23] and Lyapunov exponent spectrum [24] from observed time series allows to overcome this difficulty to some extent.

To calculate major Lyapunov exponent we used our program. It operates according to an algorithm described in Kantz's paper. To calculate Lyapunov exponent spectrum we have used a program from "TISEAN" package, which is available at http://www.mpipks-dresden.mpg.de/~tisean/.

Unfortunately, for a TWT-generator calculation of Lyapunov exponents requires considerable time, and results turn out to be sensitive to parameters of calculation procedure, even with application of mentioned algorithms.

4. THE RESULTS OF ANALYSIS OF CHOSEN MODELS OF GENERATORS

4.1. Dynamics of the system based on traveling-wave tube

Control parameter for a model of TWT-generator is parameter ε featuring pass-band of low-frequency filter. In the beginning, parameters α and β, determining gain factor and degree of asymmetry of nonlinear characteristics were fixed. As can be seen in bifurcation diagram in Fig. 10, the system undergoes a series of period doubling bifurcations as control parameter decreases. After the series of bifurcations chaotic modes follow. Their complexity, as is shown below, increases with decreasing of the control parameter. The smaller ε the more the band pass is, and, correspondingly, the richer the dynamics is. This can also be seen in the bifurcation diagram.

Fig. 10 also shows results of estimation of Lyapunov exponent spectrum for five-dimensional embedding space. As has already been noted, calculation of Lyapunov exponent spectrum is a complex task, and results are sensitive to algorithm's details. So, the role of Fig. 10 is not to give exact values of Lyapunov exponents, but rather to show regions where one or both Lyapunov exponents are positive. Regions of hyperchaos, where two or more Lyapunov exponents are positive, have complex dynamics and are not considered here. We pay attention to relatively simple low-dimensional modes, with one positive Lyapunov exponent – modes with control parameter values between 0.4 and 0.45.

Figures 11-15 represent waveforms, spectra and calculated embedding space dimensions by method of Karhunen-Loeve (right in figures). Values of control parameter between 0.75 and 0.5 correspond to periodic motion. As can be seen from the spectrum of eigenvalues of covariance matrix (result of calculation of embedding space dimension), two first eigenvalues differ substantially from the others. One may surmise that two-dimensional space is enough to describe these modes.

For more complex modes, for instance, for the mode with ε=0.444, the difference between pairs of eigenvalues is already smaller. In practice we use three-dimensional embedding space for such modes.

Figures 16 and 17 show results of calculation of correlation dimension for the above modes. Apparently, for $\varepsilon = 0.1$ dimension exceeds 5 and saturation does not take place even for embedding space dimension equal to 10. Such modes are not considered here.

For a mode with $\varepsilon = 0.4$ an estimate of correlation dimension is between 2.5 and 3, and saturation takes place when embedding space dimension equals three. In the following section we make at attempt to construct symbolic description for relatively low-dimensional modes in the range 0.4...0.45. As is shown below, symbolic description could be constructed only in rather narrow region of parameters.

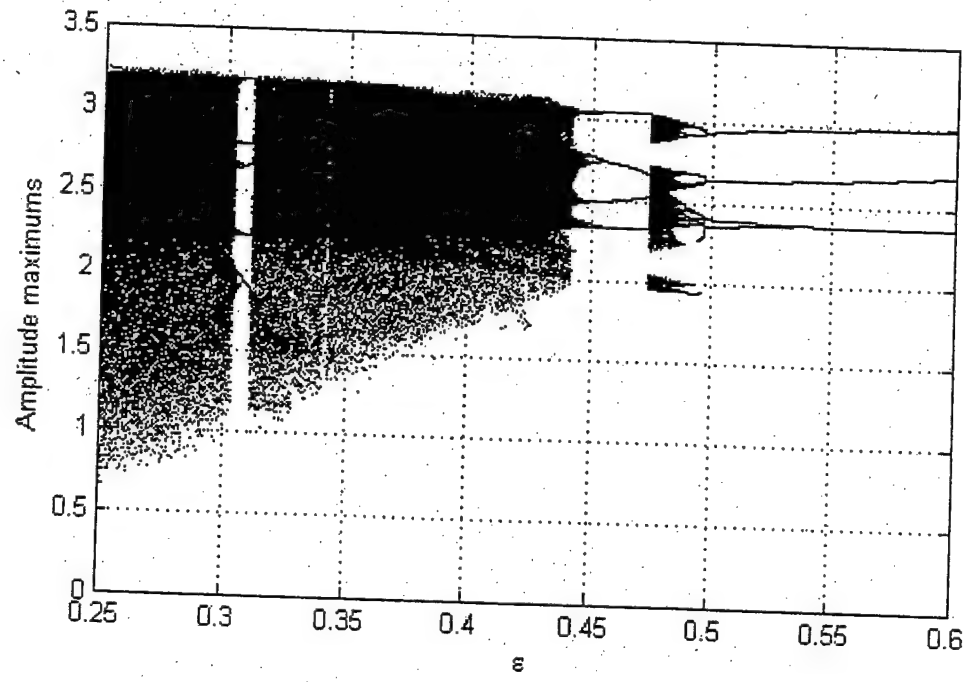

(a)

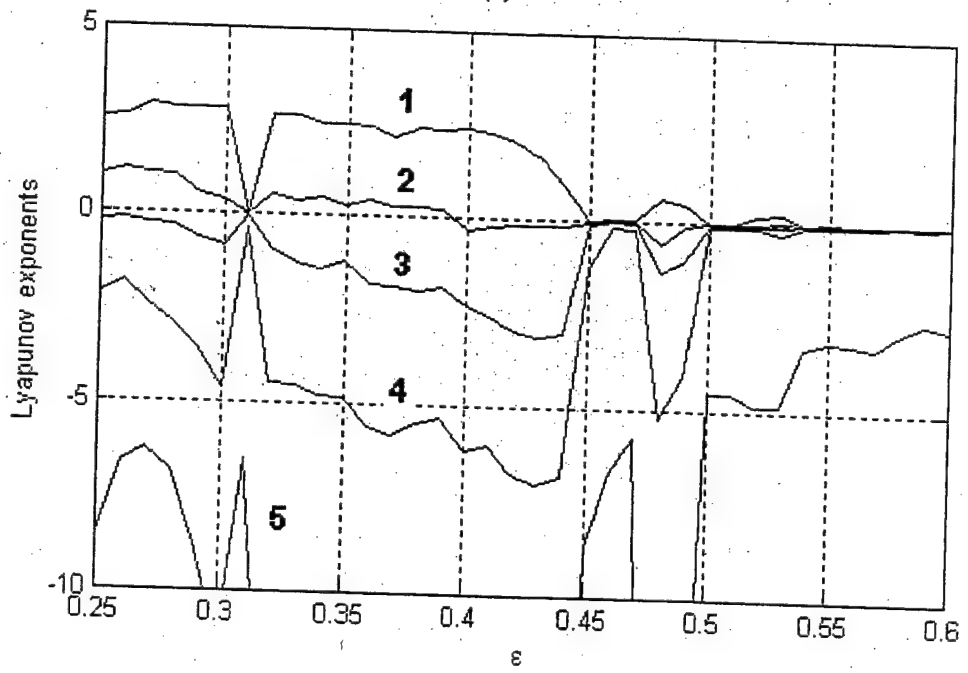

(b)

Fig. 10 Bifurcation diagram (a) and Lyapunov exponents spectrum (b) for the model of TWT-generator (curves 1,2,3,4,5 correspond to the first five Lyapunov exponents)

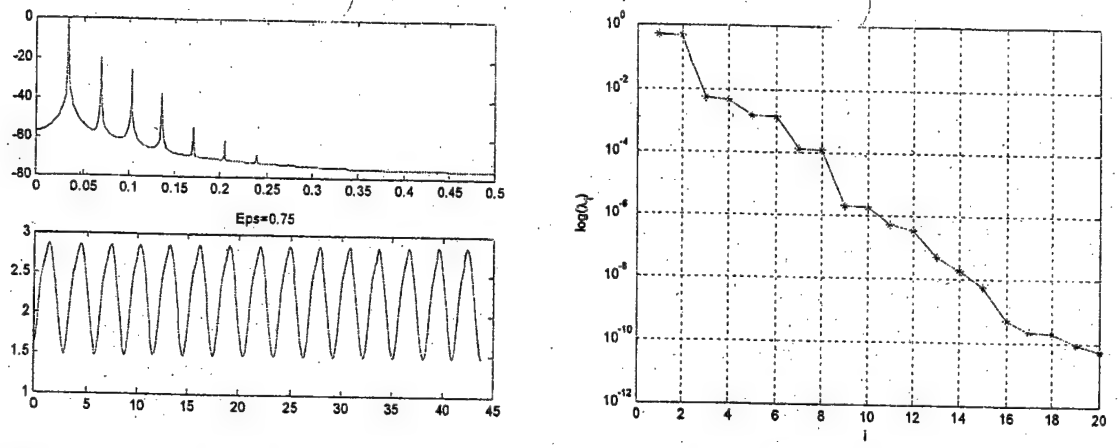

Fig. 11. Power spectrum, waveform and spectrum of eigenvalues of covariance matrix for system (8) at $\alpha = 2.05$, $\beta = 1.45$, $\varepsilon = 0.75$.

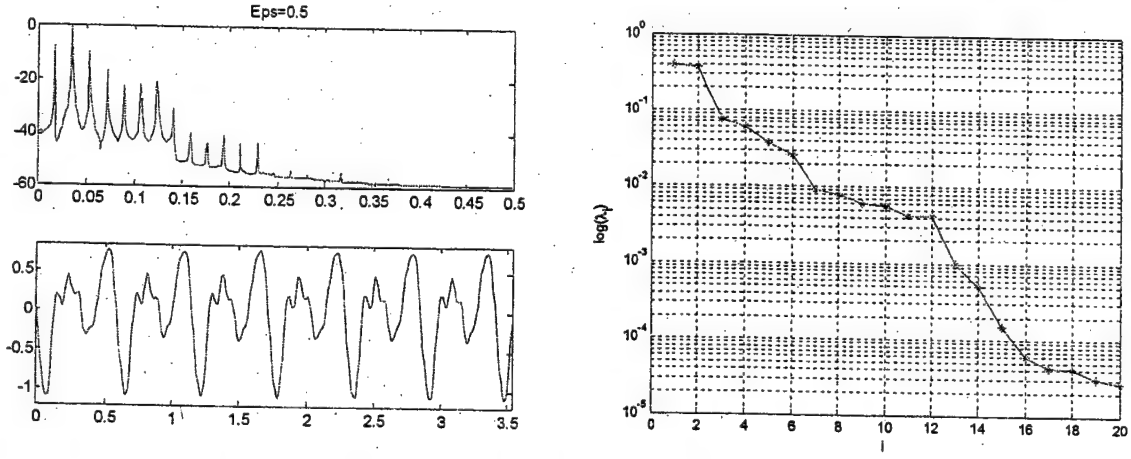

Fig. 12. Power spectrum, waveform and spectrum of eigenvalues of covariance matrix for system (8) at $\alpha = 2.05$, $\beta = 1.45$, $\varepsilon = 0.5$.

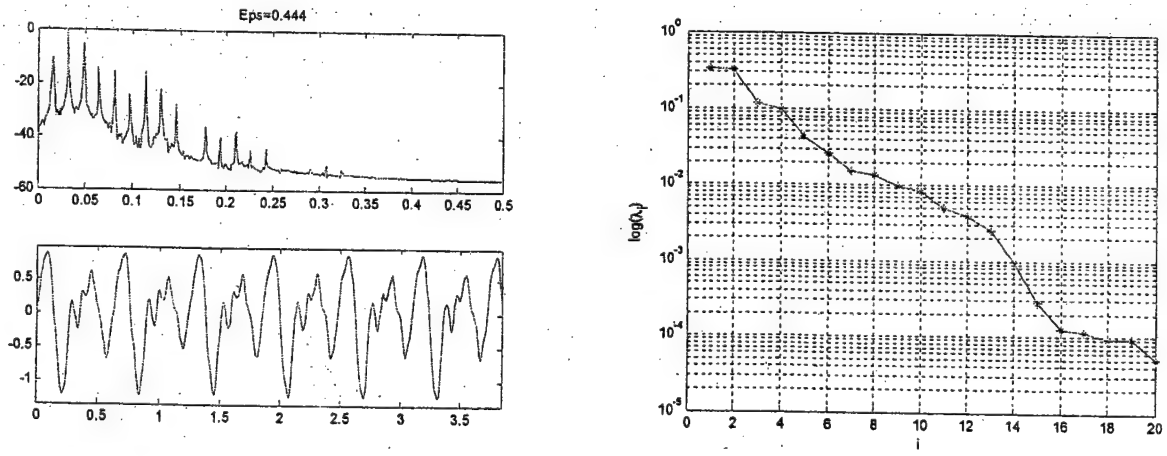

Fig. 13. Power spectrum, waveform and spectrum of eigenvalues of covariance matrix for system (8) at $\alpha = 2.05$, $\beta = 1.45$, $\varepsilon = 0.444$

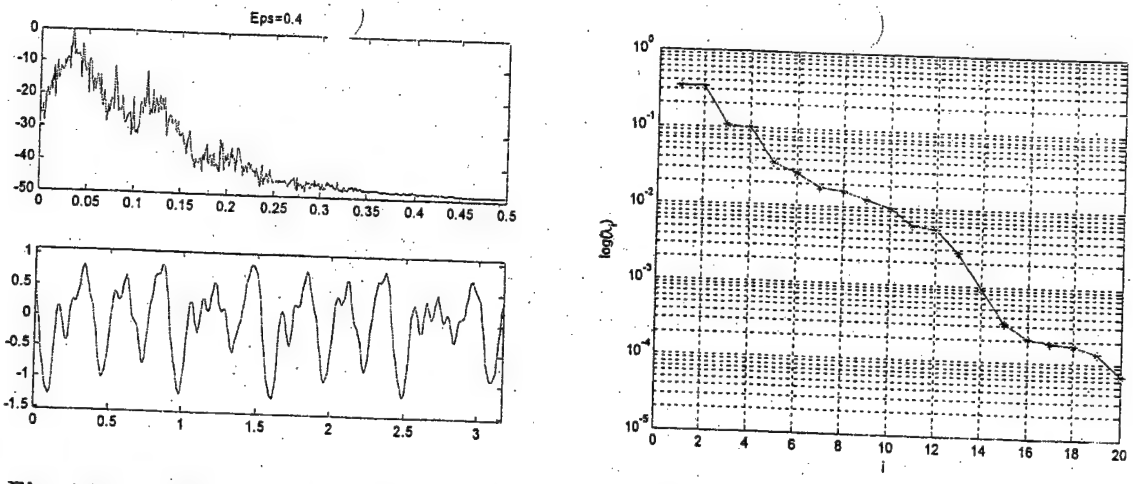

Fig. 14. Power spectrum, waveform and spectrum of eigenvalues of covariance matrix for system (8) at $\alpha = 2.05$, $\beta = 1.45$, $\varepsilon = 0.4$

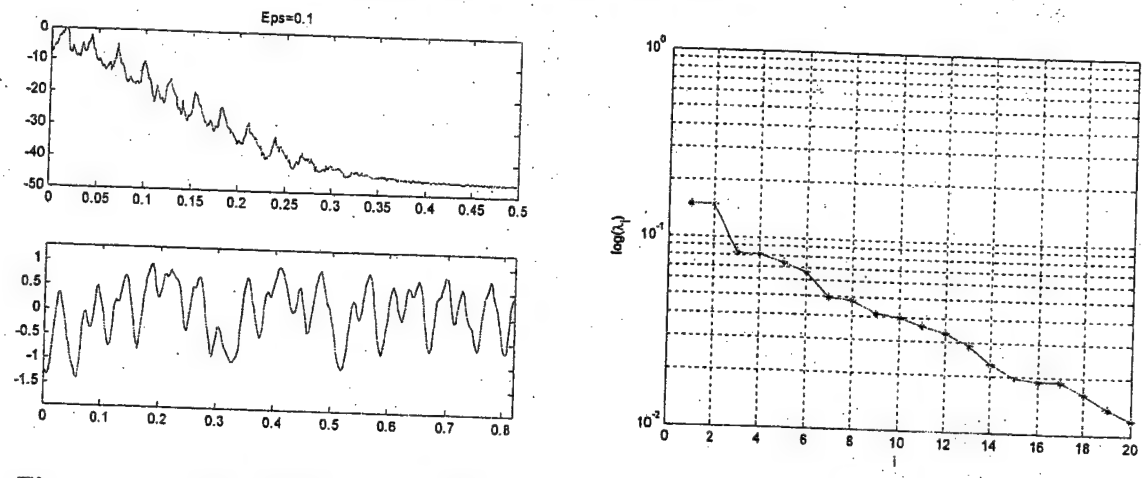

Fig. 15. Power spectrum, waveform and spectrum of eigenvalues of covariance matrix for system (8) at $\alpha = 2.05$, $\beta = 1.45$, $\varepsilon = 0.1$

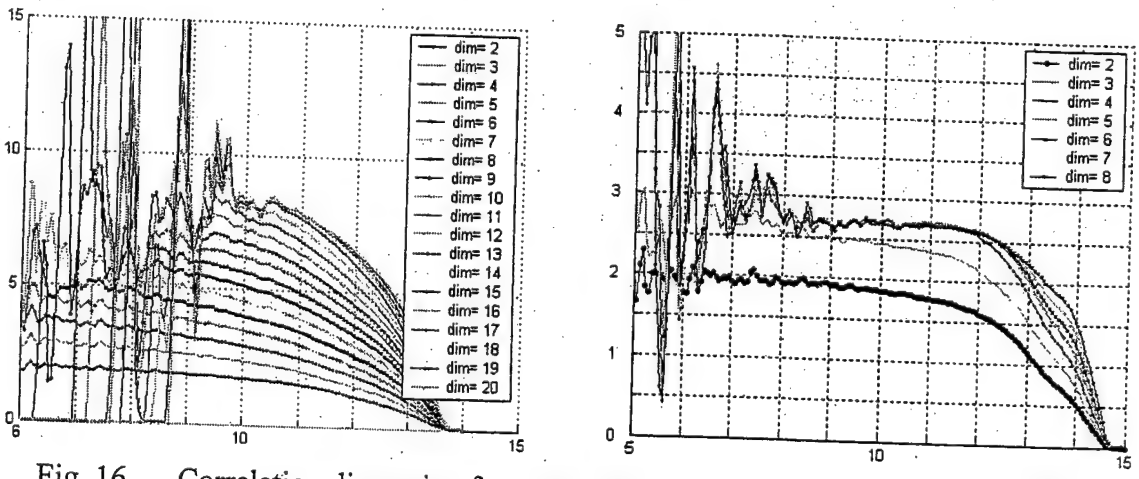

Fig. 16. Correlation dimension for system (8) at $\alpha = 2.05$, $\beta = 1.45$, $\varepsilon = 0.1$ (left) и $\varepsilon = 0.4$ (right)

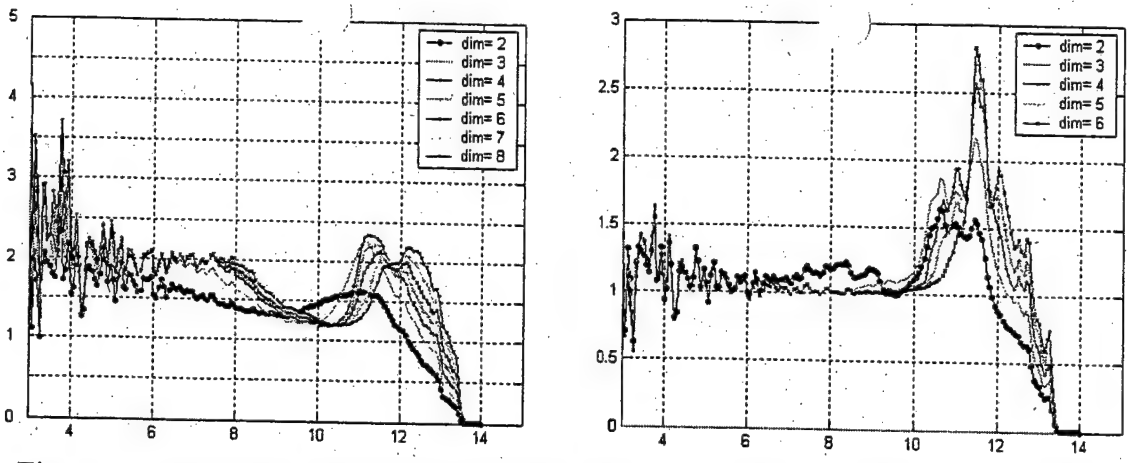

Fig. 17. Correlation dimension for system (8) at $\alpha = 2.05$, $\beta = 1.45$, $\varepsilon = 0.1$ (left) и $\varepsilon = 0.5$ (right)

4.2. Dynamics of the microtriode generator.

Control parameters of generator based on microtriode (14) are V and p. Fig. 18 shows bifurcation diagram and Fig. 19 shows the major Lyapunov exponent as a function of parameter V in the range [0.18...0.24].

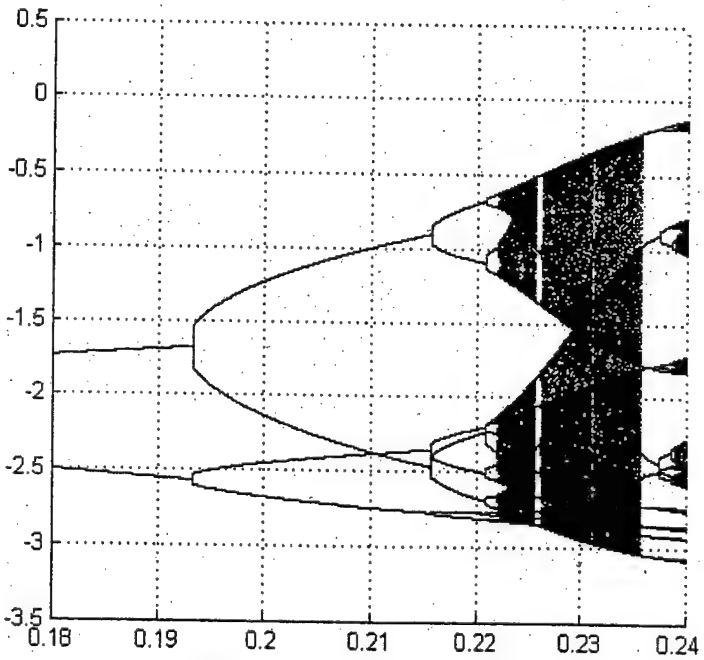

Fig.18. Bifurcation diagram for system (14).

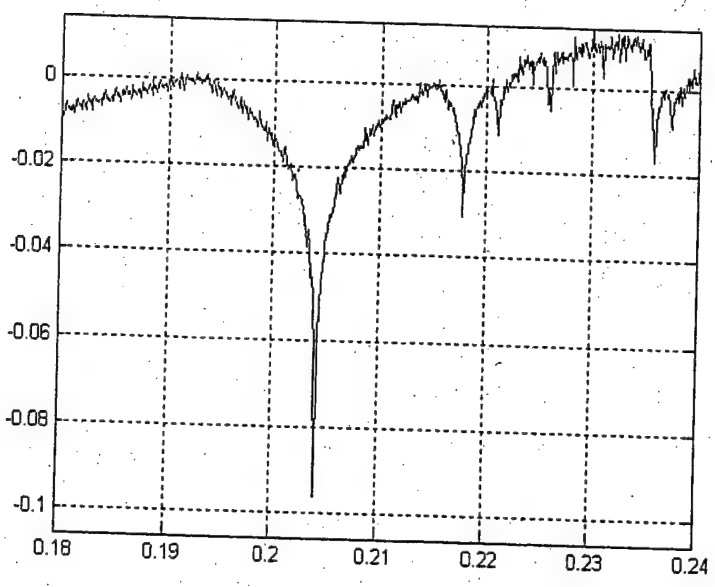

Fig.19. Diagram of major Lyapunov exponent for system (14).

Both the bifurcation diagram and the Lyapunov exponent indicate that a region of parameters exists where the system demonstrates chaotic behavior. In the next chapter we construct symbolic dynamics for this system for parameter values V between 0.222 and 0.233.

As an example, Fig. 20 shows the signal and spectrum of chaotic mode of system (14).

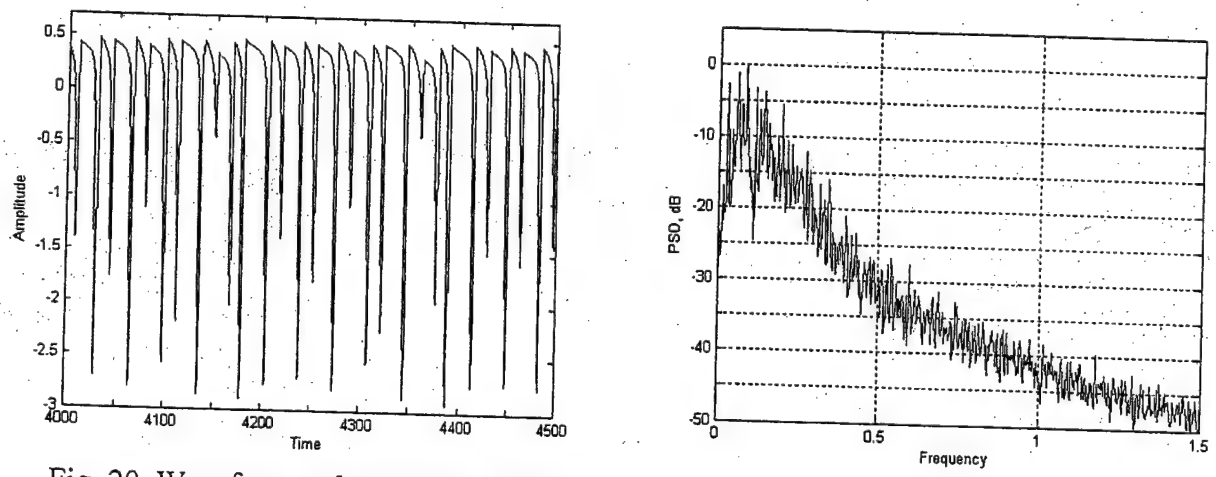

Fig. 20. Waveform and spectrum of signal of system (14) for control parameter $V = 0.23$.

Oscillations in system (14) are of relaxation type, which leads to strong spectrum spreading, even for periodic modes.

5. ALGORTIHM FOR CONSTRUCTION OF SYMBOLIC DESCRIPTION

In this section we demonstrate that in some modes, continuous signals generated by discussed generators could be associated with binary symbolic sequences.

Let us give basic definitions of the terms used.

Let a map be given by:

$$x_{n+1} = f(x_n),\ x_n \in G \subseteq R^N, \tag{20}$$

where R^N is N-dimensional real space; G – a set in R^N, where the map (20) is defined.

Any set of m non-overlapping regions $\beta=\{B_i\}_{i=1}^{i=m}$, which covers set G of dynamic system states, is called partition

$$\beta=\{B_i\}_{i=1}^{i=m}:\ B_i \cap B_j = \varnothing \text{ for } i \neq j;\ \bigcup_{i=1}^{i=m} B_i = G. \tag{21}$$

Let us introduce a symbol $i = \xi(B_i),\ i \in M = \{1,2,3,\ldots m\}$ for every region B_i of partition β. Let then denote a set of all sequences of unbounded length $X_1^\infty = X_1X_2\ldots X_j\ldots$, with $X_j \in M$, as $\Psi = \prod_{i=1}^{\infty} M$. Thus we get a map $\mu_\beta : G \to \Psi$

$$\mu_\beta(x_1) = X_1^\infty \Leftrightarrow f^{j-1}(x_1) \in B_{Xj} \text{ for } j \geq 1, \tag{22}$$

which relates a sequence $X_1^\infty \in \Psi$ to every point $x_1 \in G$, where X_j is a symbol generated at time j. Sign $\Leftrightarrow$ means an equivalence between the sequence X_1^∞ and a sequence of samples obtained after iteration of the map $f(x_1)$.

According to (22) the dynamics, defined by a map f in the phase space, is translated to a set of symbolic sequences Ψ based on alphabet M. In such manner a symbolic dynamic system is a left-shift homomorphism. $\hat{\sigma}$ is formed: $\hat{\sigma}(X_1^\infty)_i = X_{i+1}$, (where X_i – i-th symbol in X_1^∞). A set $L \subseteq \Psi$ of all sequences, generated by the system, is called a *language*. The study of symbolic dynamic system $(\Sigma_L, \hat{\sigma})$, where Σ_L – is a set of all unbounded sequences compatible with L, is equivalent to the study of the map, provided that partition of f is *generating*, i.e. if every unboundedly long symbolic sequence corresponds to the unique initial condition x_1.

The motion of dynamic system in continuous (microscopic) state space is determined and described by equation (20). If an initial state x_1 and map f are known, then future evolution of (20) might be calculated. On the contrary, the motion of the system on partition (macroscopic motion) is stochastic, and trajectories are sequences of symbols. If a past trajectory of equation (20) on the partition is known, it is possible to predict its future macroscopic states only in probabilistic terms. Different states which belong to the same region B_{Xj} at time j, could get into different regions at time $j+1$ because of stochastic nature of dynamic system. State space partition transforms a determined system into a source of information (messages), which could be analyzed in terms of information theory. The entropy could be derived for such source of messages:

$$H_n^\beta = -\sum_{X_1^n} P(X_1^n)\log_2 P(X_1^n), \tag{23}$$

where $P(X_1^n)$ is probabil.. of the trajectory fragment (word) X_1^n $X_1X_2...X_n$. H_n^β determines average uncertainty for prediction of a word of length n. For the case of known past n symbols, a conditional entropy of $(n+1)$ symbols in macroscopic trajectory equals

$$h_n^\beta = H_{n+1}^\beta - H_n^\beta, \text{ where } n = 1,2,... \text{ and } h_0^\beta = H_1^\beta. \quad (24)$$

The rate of entropy production by a source (20) for this partition β is determined by the expression

$$h^\beta = \lim_{n\to\infty} h_n^\beta = \lim_{n\to\infty} \frac{1}{n} H_n^\beta. \quad (25)$$

Kolmogorov entropy (K-entropy) of an equation (20) is an upper limit of the rate of entropy creation by a source for all possible partitions:

$$h_K = \sup_\beta h^\beta. \quad (26)$$

If $h^\beta = h_K$, then β is a generating partition. An interesting property of generating partition is that corresponding map (22) is reversible, i.e. if initial conditions do not coincide, then symbolic sequences would be different: from $x' \neq x'' \Rightarrow \mu_\beta(x') \neq \mu_\beta(x'')$.

In order to map a continuous trajectory into a symbolic sequence the continuous trajectory is transformed into a discrete one by introduction of Poincare section Σ (succession map). Then consecutive intersections of the trajectory with Σ are considered. The section plane Σ is selected individually for every system, and not all points of crossing of the trajectory with Σ are used but only those where the trajectory crosses the plane in particular direction.

Let illustrate this for the Rossler system (15) with parameter values $a = 0.15$, $b = 0.2$, $c = 10$.

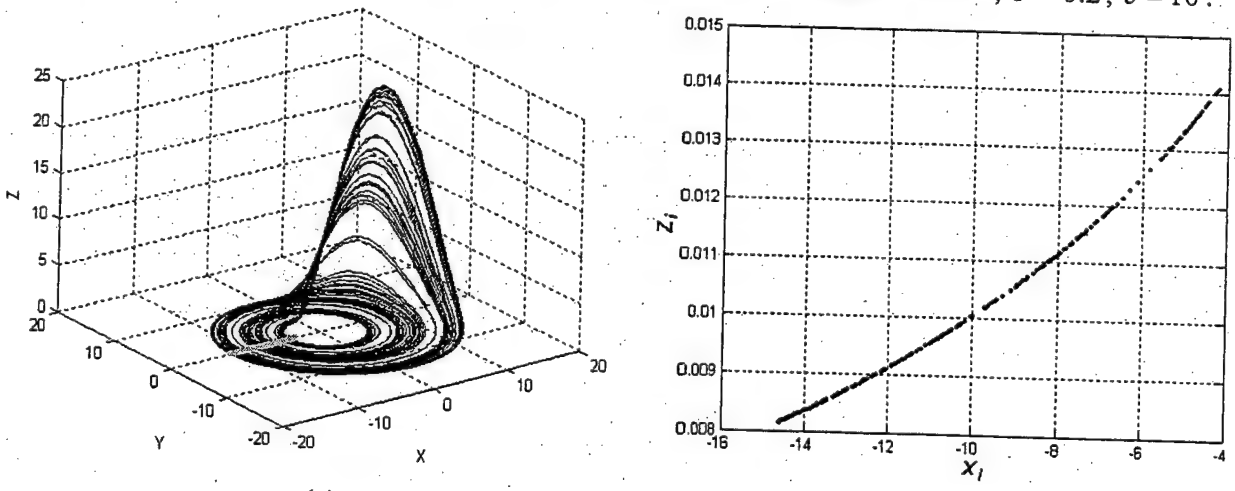

(a) (b)

Fig. 21. Phase portrait for Rossler system (15) (left) and points $\mathbf{x}_n=(x_n, z_n)$ of crossing of the trajectory with the plane $y = 0$

Three-dimensional phase portrait of the system for such parameter values is depicted in Fig. 21a. For this case, a convenient choice of the section plane would be $\Sigma = \{(x,z): y = 0; x < 0\}$. Second condition accounts for the shape of the attractor in the XY projection and general direction of the flow.

In this case crossings of the trajectory with Σ take place at $\dot{x} = 0$ and $\ddot{x} < 0$. A map in section plane Σ introduced in this way is

$$x_{n+1} = F(x_n) \tag{27}$$

where x denotes location of a vector on Σ, n *is* discrete time, F: Σ→Σ nonlinear function, which is unknown in general case. Map (27) for Rossler system is depicted in Fig. 21b, where $\mathbf{x}_n=(x_n,z_n)$. Such dependence $z_n(x_n)$ is a result of a good choice of the section plane and the simplicity of the Rossler system dynamics for given parameter values. For other section planes Σ the dependence $z_i(x_i)$ might become more complex, and, in particular, lose unambiguity in the projection at one or both of the axes.

Note that thorough consideration of symmetries and local direction of the flow should be done separately for every system under consideration. However, experimentally observed low-dimensional attractors frequently have a simple (single-loop) structure and choice of Poincare sections does not present difficulties.

In order to get a symbolic encoding of the motion on attractors of map F (27), a section Σ is divided by a finite number b of non-overlapping regions B_k, with $k \in M = \{0, 1,\ldots b\text{-}1\}$, which cover region, where an asymptotic behavior take place. Consequently, a set $\beta = \{B_k\}$ is a partition. Every trajectory $\mathbf{O} = \{x_1, x_2,\ldots x_n\}$ is associated with symbolic sequence $S = s_1 s_2 \ldots s_n$, which consist of labels s_i of regions B_{Si}, which are visited at time $i = 1, 2, \ldots n$. In turn, subregions are indexed by combinations of symbols $S = s_k s_l \ldots$, and all combinations begin from the label s_k of parental set B_{Sk}: thus, for instance, all points in an element B_{S1S2} belong to B_{S1} at time $i = 1$ and would be mapped into regions B_{S2} at time $i = 2$. All points x in B_S produce the same symbolic trajectory S under the effect of F before the expansion into different regions of β.

Generating partition could be constructed in a systematic way in hyperbolic systems where stable and unstable manifolds intersect transversally in every point. It is not clear, however, how to identify a generating partition for "general" non-hyperbolic dynamics, which are characterized by tangency between stable and unstable manifolds and absence of exponential repulsion in certain regions of phase space (that corresponds to negativity of all Lyapunov exponents calculated on finite part of a trajectory). Non-hyperbolic motion is typical for real-world systems.

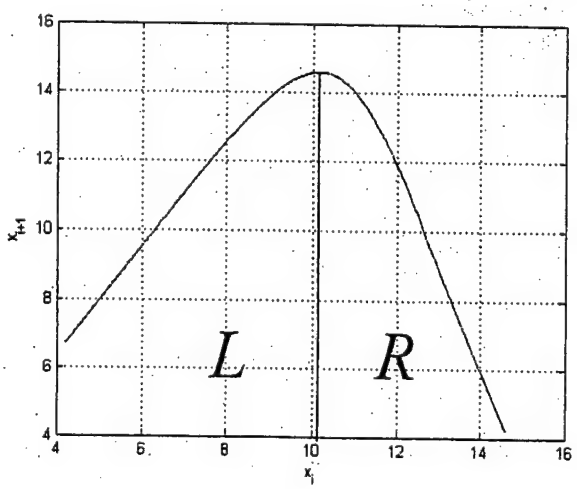

Fig. 22. Quasi-one-dimensional map $x_{i+1}(x_i)$ for system (15) and generating partition

In the example with Rossl ystem, a generating partition is introd. d through transition to one-dimensional map by one coordinate, for example $x_{i+1}(x_i)$. This dependence is depicted in Fig. 22.

As one can see, this dependence is a one-dimensional map (or, more precisely, quasi-one-dimensional unimodal map), which is visually similar to logistic map.

As is known [28], a symbolic description can be constructed by partitioning of the plane by vertical line crossing the maximum of the map. If a value x_i is to the left from the vertical line, then the value of the i-th element of the symbolic sequence is L (or «0»). If value x_i is to the right from the vertical line, then the i-th element of the symbolic sequence is R (or «1»).

The waveform of X is depicted in Fig. 23 and the line corresponding to generating partition (Fig. 22) is plotted. Local minima above the line correspond to symbols "L" or "0" and local minima below the line to symbols "R" or "1".

Thus, the procedure of construction of symbolic description is as follows. A discrete vector sequence (x_i, y_i, z_i) is formed from continuous chaotic trajectory by means of Takens procedure. Then, some coordinate x of this sequence is considered and the dependence $x_{i+1}(x_i)$ is plotted. If this plot turns out to be a quasi-one-dimensional unimodal map, then it is possible to define a generating partition: values x_i are associated with symbols L or R («0» or «1»), depending on whether the sample x_i is on the left or on the right from the extremum:

$$s_i = \begin{cases} L, \ if \ \ x_i < x_{top} \\ R, \ if \ \ x_i > x_{top} \end{cases} \qquad (28)$$

As a result, binary symbolic sequence s_i is associated with continuous chaotic trajectory $x(t)$.

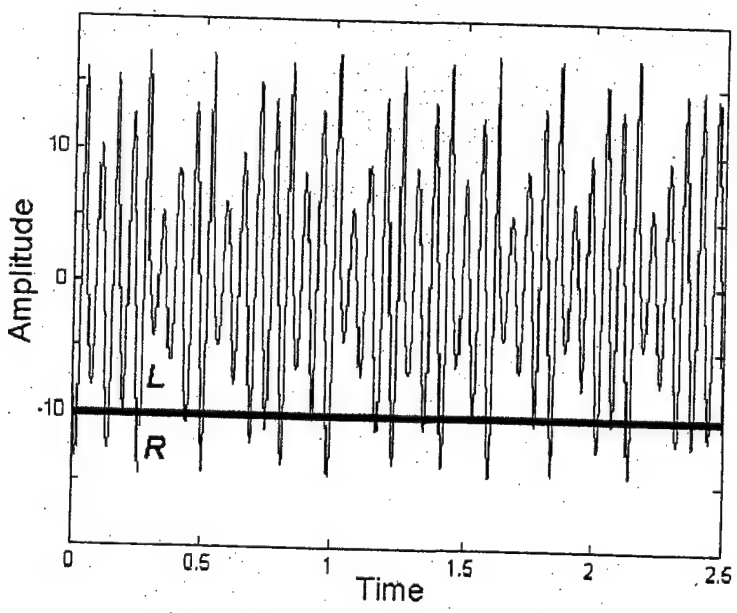

Fig. 23. Generating partition and X waveform of Rossler system.

As can be shown if equations of the system and symbolic sequence are known, then a chaotic trajectory can be reconstructed, in principle, with arbitrarily high precision. Algorithm for reconstruction is described in detail in the next section for the system based on microtriode.

Note that in general case s. bolic sequence does not have to be l ry for a system with rather complex dynamics. But the scope of this work is deliberately limited to the simple case of binary sequences.

A review of methods for construction of symbolic dynamics and symbolic partition can be found in [13, 25–27]. In general case construction of symbolic description is rather complex. It can be solved only in a limited number of cases.

In section 5.2 we show that for a system based on microtriode a constructed sequence is symbolic and could be used to reconstruct (with arbitrarily high precision) the initial continuous chaotic signal. Thus we find such a partition of the phase space that the obtained sequence (sequence of symbols L, R or 0,1) corresponds one-to-one to continuous signal.

A similar result can be obtained for generator based on traveling-wave tube.

5.1. Symbolic description for microtriode system

Symbolic description of phase trajectory for a system based on microtriode is carried out practically in the same way as for the Rossler system, but the succession map is replaced by the shift map because the system is not autonomous.

A shift map is constructed by means of sampling the coordinates over time intervals equal to the period of external force. Namely, if T is the period then a discrete vector sequence:

$$(x_i, y_i) = (x(t_0 + iT), y(t_0 + iT)), \tag{29}$$

is associated with continuous trajectory $(x(t), y(t)) = (x(t), \dot{x}(t))$, where t_0 is some initial time offset.

Fig. 24 shows a shift map for the trajectory of microtriode generator with parameters $p = 0.18$, $s = 4.5$, $k = 10$, $g_0 = 0.54$, $m = 0.2$, $V = 0.233$.

As one can see, the shift map is a single-valued curve, as in the case of Rossler system.

Fig. 24b shows more clearly where the points of shift map lie on the phase portrait. Quasi-one-dimensional map $x_{i+1}(x_i)$ (fig. 24d) is unimodal similar to the Rossler system.

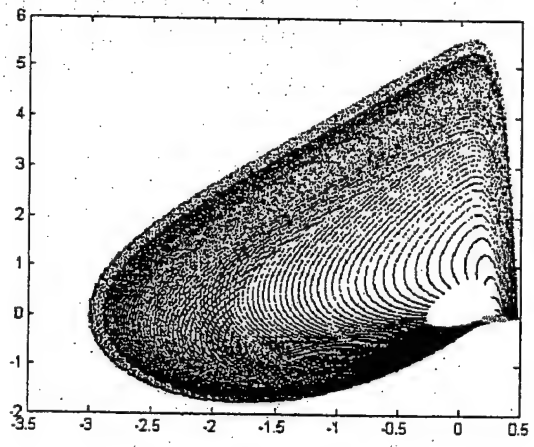

(a)

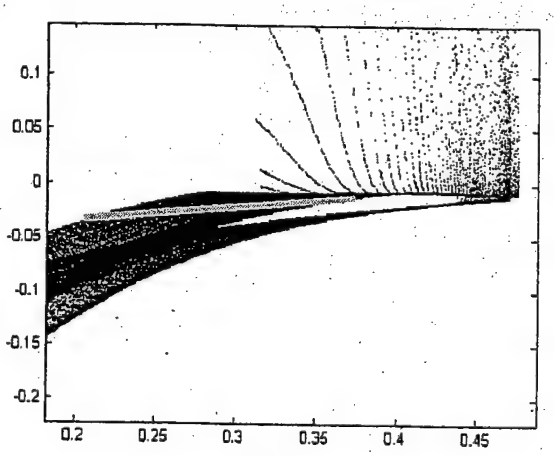

(b)

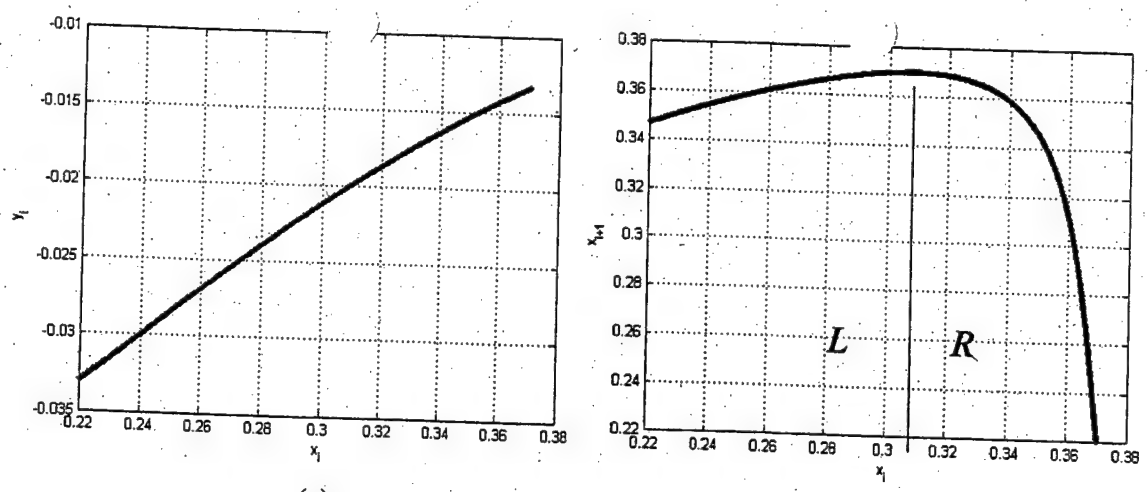

(c) (d)

Fig. 24. Shift map on the phase portrait (a); magnified shift map (b) and (c); quasi-one-dimensional map $x_{i+1}(x_i)$ for mode with $V = 0.233$ (d) in (14).

A binary symbolic sequence is constructed from a quasi-one-dimensional unimodal map, as for Rossler system. This sequence is associated with initial continuous chaotic trajectory. A chaotic trajectory could be reconstructed from this symbolic sequence with arbitrarily high precision.

Principal steps of such reconstruction are as follows.

Let a symbolic sequence $s_1, s_2, \ldots$ of binary samples and the system of equations corresponding to investigated models of chaotic oscillator be known.

1. As is shown in [29] for unimodal one-dimensional map $x_{i+1} = f(x_i)$ sample values x_i can be reconstructed from symbolic sequence $\{s_i\}$ with arbitrarily high precision. It can be reconstructed owing to knowledge about future values of symbolic sequence s_i. The more elements N of symbolic sequence is used for reconstruction, the higher precision of reconstruction of x_i is. Precision of reconstruction depends exponentially on number N of used elements of symbolic sequence. In the case of microtriode the only difference here is that map f is not given explicitly. It can be obtained only approximately based on calculation of long trajectory. The key point here is that it is sufficient to calculate a map one time with necessary accuracy. Then the map could be reused repeatedly. Details on this stage of the algorithm, its implementation and complications can be found in [29]

2. Having obtained values x_i it is possible to obtain value y_i by means of Poincare map (shift map) (Fig. 24) which is known numerically.

3. Pairs (x_i, y_i) can be used as initial conditions for integration of the system on time interval equal to the period of external force. Thus, from known (x_1, y_1) we get approximate continuous trajectory on $[0, T]$. Known (x_2, y_2) gives us approximate continuous trajectory on $[T, 2T]$, and so on. Such trajectory can be discontinuous at moments of transition to new initial conditions, but these discontinuities can be made arbitrarily small by more precise calculation of points (x_i, y_i).

Fig. 25 shows the differen[ce] between the initial chaotic signal and [the] signal reconstructed from symbolic sequence for the cases of $N = 50$ and 200 elements of symbolic sequence s_i used for reconstruction of each point x_i.

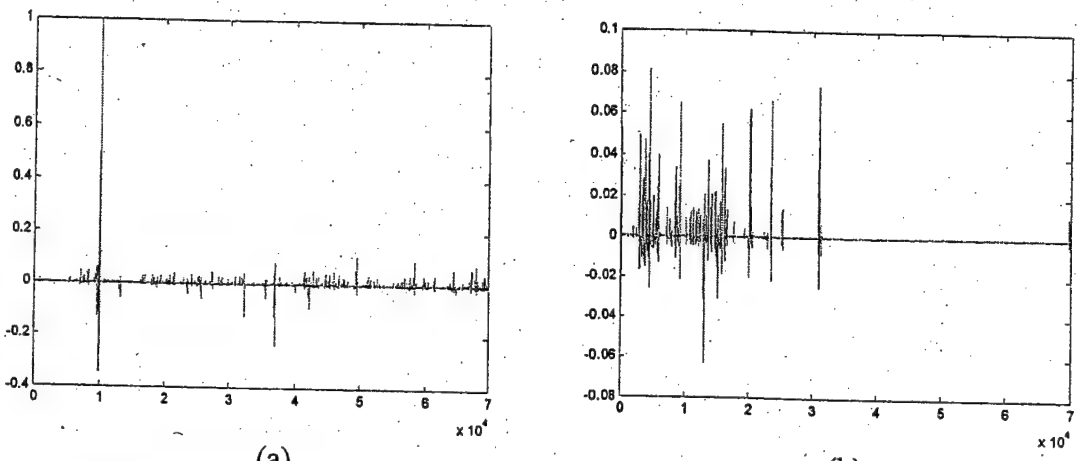

(a) (b)

Fig. 25. Difference between the initial chaotic signal and the signal reconstructed from symbolic sequence: (a) the length of symbolic sequence is $N = 50$ symbols and (b) $N = 200$ symbols.

For bigger N it is possible to reconstruct a trajectory *perfectly exactly*, i.e. with precision of computer calculations.

Dispersion σ of difference between the initial and reconstructed sequences as function of N is shown in Table 1.

Table 1

σ	0.014	0.006	0.004	0.002	0.0007
N	50	100	150	200	300

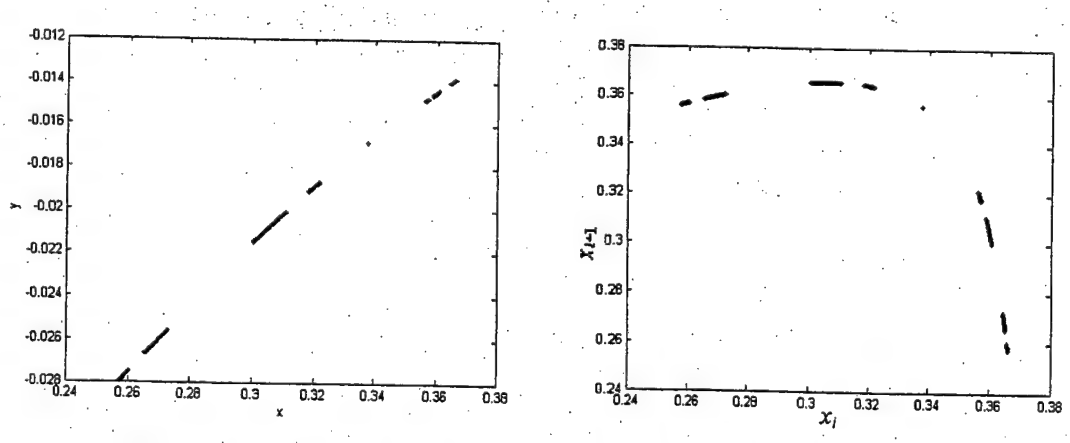

Fig. 26. Shift map and quasi-one-dimensional map $x_{i+1}(x_i)$ for (14) with $V = 0.222$.

At this point we have shown an algorithm for construction of symbolic sequence and reconstruction of chaotic trajectory from symbolic sequence only for a particular set of parameters.

However, as numerical exp nents indicate, the shape of Poincare . p and unimodal quasi-one-dimensional map practically do not change for different values of V. Fig. 26 shows these maps for weakly chaotic mode V=0.2221. As one can see, only a degree of filling the curve by points is changing. Even the coordinate of the maximum remains the same.

Since not all symbolic sequences are possible, we have analyzed which symbolic sequences are permitted and which are prohibited. For this purpose we constructed and analyzed a symbolic sequence for long chaotic trajectory.

The results are reported as histograms for modes with V=0.233 and V=0.225. Fig. 27 shows histograms demonstrating which sequences of length two are permitted by generator dynamics. Sequences are numerated by natural numbers, correspondence is indicated in Table 2. Index of a sequence is simply decimal form of its numerical value, if the sequence is treated as a as binary number.

Table 2

Sequence	Number
LL (00)	0
LR (01)	1
RL (10)	2
RR (11)	3

As one can see in Fig 27, a sequence with number 0, i.e. sequence LL, is prohibited in these modes.

So we have possibility to identify chaotic signal of particular chaotic oscillator in some practical applications. For example, if a signal comes into a receiver, and two first succession elements of corresponding symbolic sequence are L, then it is a "stranger" signal or a signal distorted in communication channel.

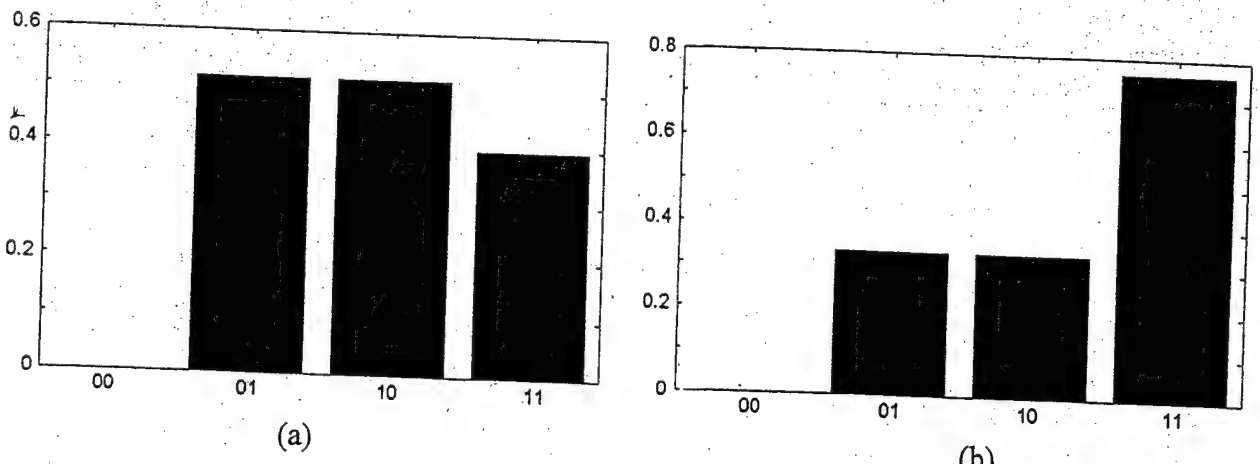

Fig. 27. Histograms of relative frequencies of permitted binary symbolic sequences of length 2 in (14) for (a) $V = 0.233$ and (b) $V = 0.225$.

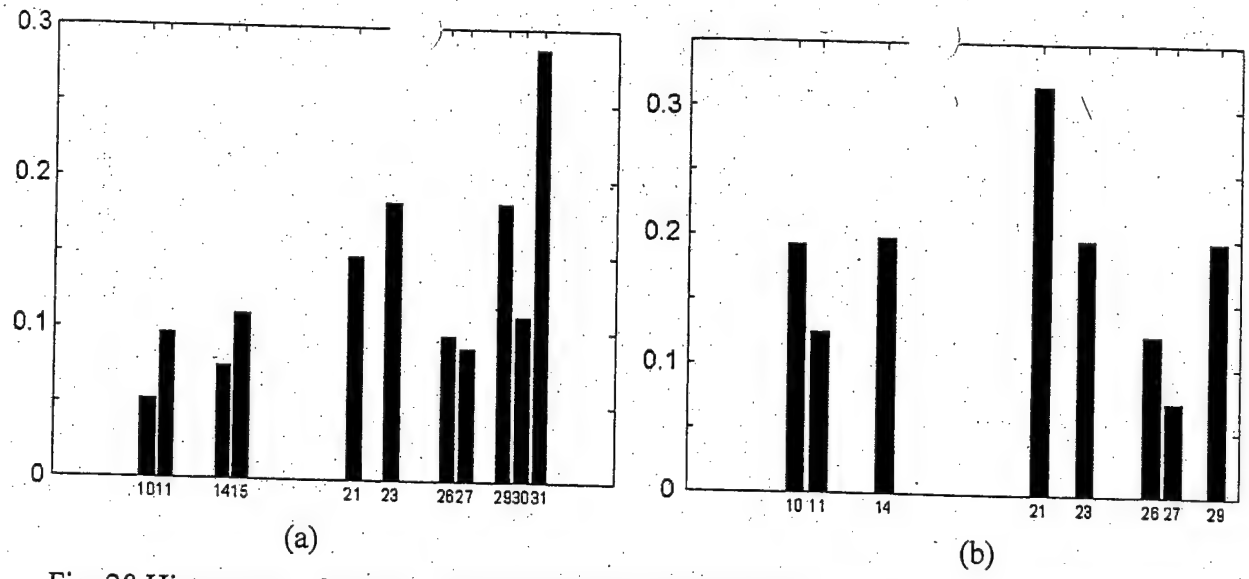

Fig. 28 Histograms of relative frequencies of permitted binary symbolic sequences of length 4 in (14) for (a) $V = 0.233$ and (b) $V = 0.225$.

Another interesting question concerns the possibility of discerning different modes of a generator based on microtriode by means of analysis of symbolic dynamics. For example, do the sets of permitted sequences differ for the modes mentioned above? To answer this question it is sufficient to analyze sequences of length four. But for better visualization we consider sequences of length five. Histograms for these sequences are presented in Fig. 28.

As one can see, in a more developed mode with $V = 0.233$ sequences are permitted with numbers 15, 30 and 31, i.e. sequences $LRRRR$, $LRRRL$ и $LRRLR$, which are prohibited for mode with $V = 0.225$. This difference enables to discern these two modes in the oscillator simply by determining prohibited sequences for the analyzed signal.

5.2. Symbolic description for TWT-system

Construction of compact information description for TWT-system (8) is a much more complex problem.

First, it is necessary to reconstruct the phase space of the system. Second, it is necessary to find a region of modes with relatively simple dynamics. Third, even for low-dimensional modes the search for convenient Poincare section, which could give good unimodal quasi-one-dimensional map, is a non-trivial task.

To construct the succession map the embedding in three-dimensional space is used. This is an essential restriction of our method.

The first method

Here an example of construction of a binary symbolic description is considered for several modes with fixed parameters $\alpha = 2.05$, $\beta = 1.45$. Parameter ε is varied in the range [0.4...0.45].

For $\varepsilon = 0.45$ a period doubling bifurcation takes place (Fig. 29). Fig. 30 shows the change of quasi-one-dimensional map $x_{i+1}(x_i)$ with decreasing of ε. Starting from $\varepsilon = 0.447$ the map becomes single-valued. (Fig. 30, 31).

The set of succession ma[illegible]epicted in Figs 29-33 show that syn[illegible]ic description for this model can be constructed only for values of control parameter corresponding to threshold of appearance of chaotic oscillations. When the driving parameter is decreased, the shape of the succession map and quasi-one-dimensional map become considerably more complex. In quasi-one-dimensional maps several additional branches arise that either require a more complex parameterization or the introduction of an additional reversible transformation of quasi-one-dimensional map to eliminate ambiguity in the projection on axes and get the possibility to construct the generating partition. Succession map depicted at Fig. 33 is one of the best maps (i.e., giving one of the most "one-dimensional", almost single-valued and almost unimodal) that we found for this mode. Because this map is not strongly single-valued, an algorithm of reconstruction of samples x_i used before is badly applicable.

An essential feature of this succession map is the presence of the third branch that favors the conclusion that symbolic description requires at least three symbols.

Nevertheless some problems described bellow can be considered even for such map.

The maximum of this quasi-one-dimensional map can be assumed to be at 1.526 so that the map consists of two monotonous branches and the generating partition can be introduced. Further estimates show that the sequence constructed in this way is in a close connection with the initial chaotic trajectory.

To show this we use the following consideration. Two close chaotic trajectories diverge with time. If symbolic sequences are constructed for these trajectories, then first several symbols coincide but from a certain moment the sequences become different. The more members of symbolic sequences coincide, the closer are the trajectories.

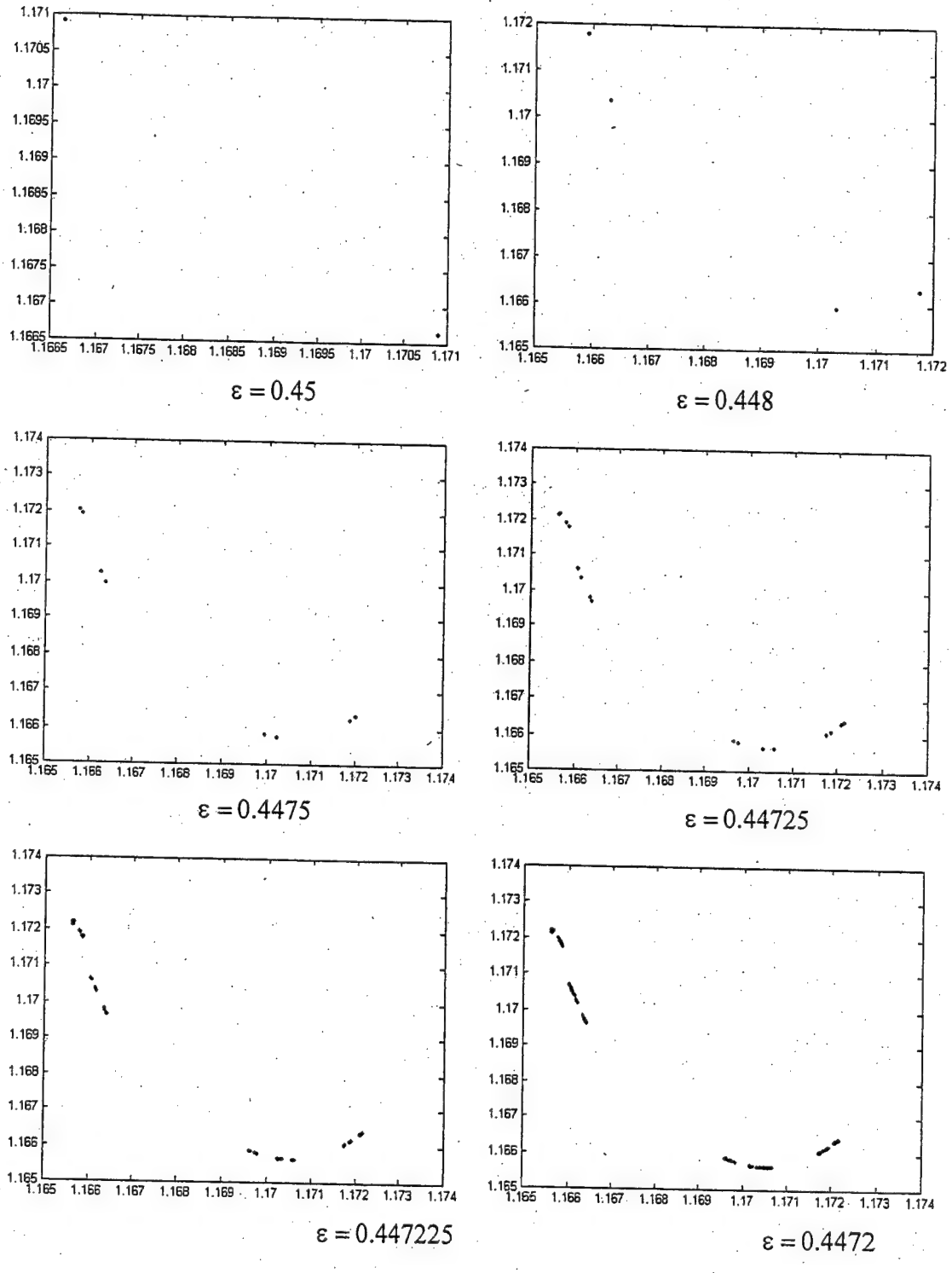

Fig. 29. Change of quasi-one-dimensional map with decrease of ε : period doubling bifurcation

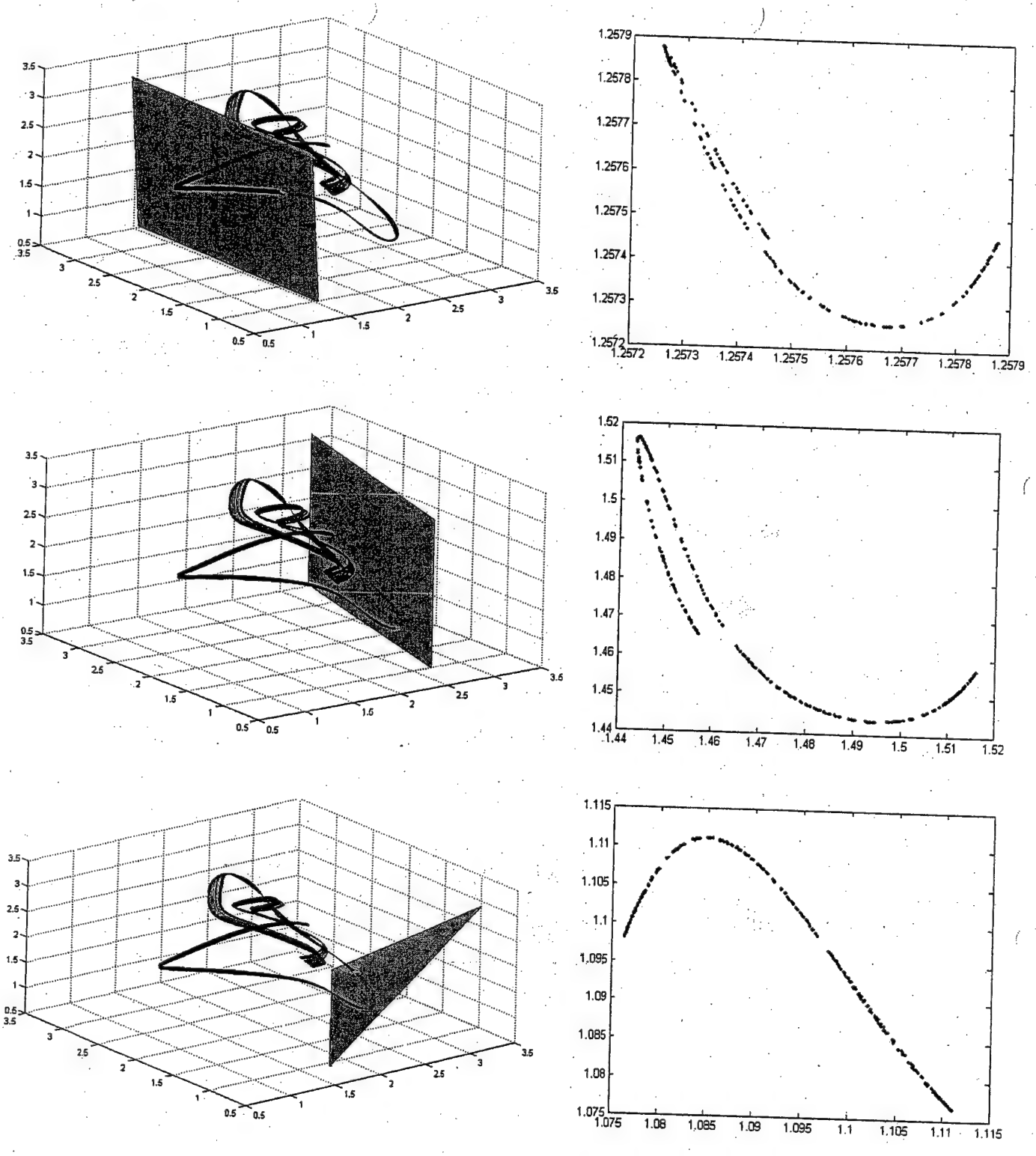

Fig. 30. Reconstructed phase portrait, Poincare section (left) and quasi-one-dimensional map for $\varepsilon = 0.446$ for different Poincare cross-sections.

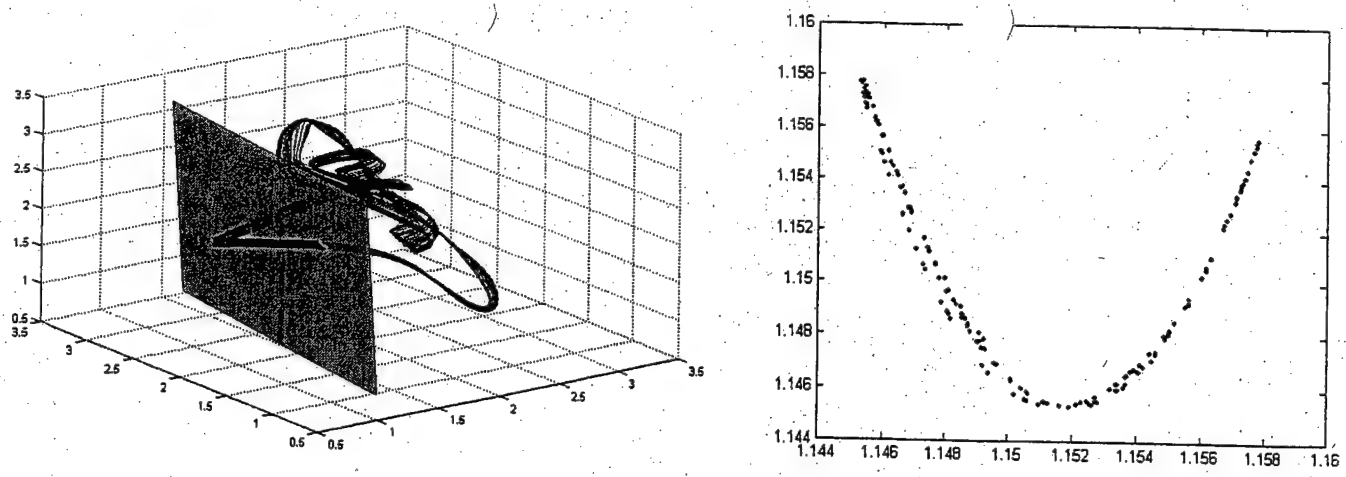

(a) ε=0.445

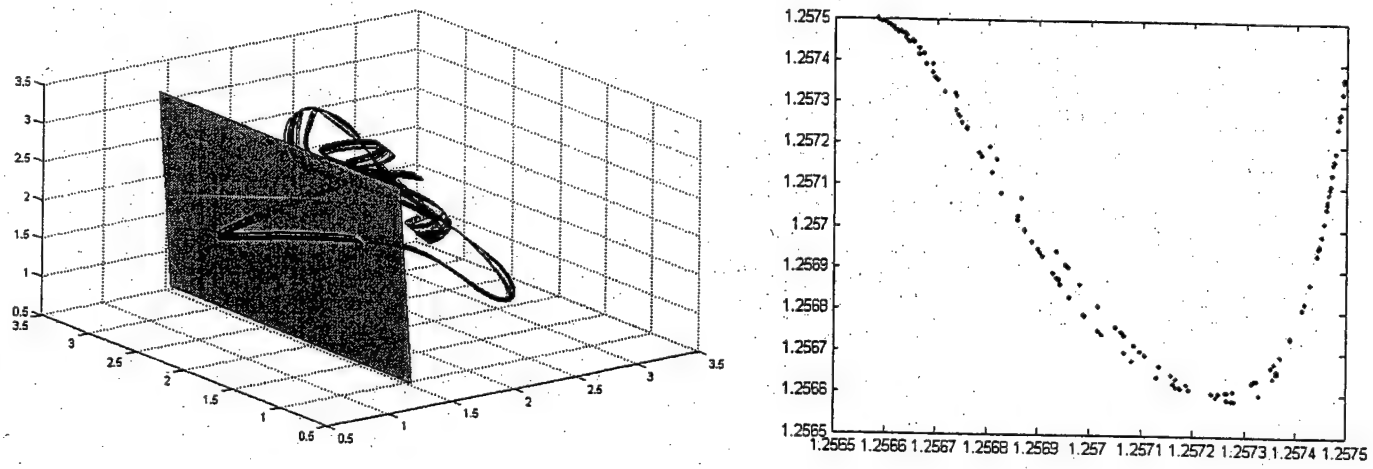

(b) ε=0.444

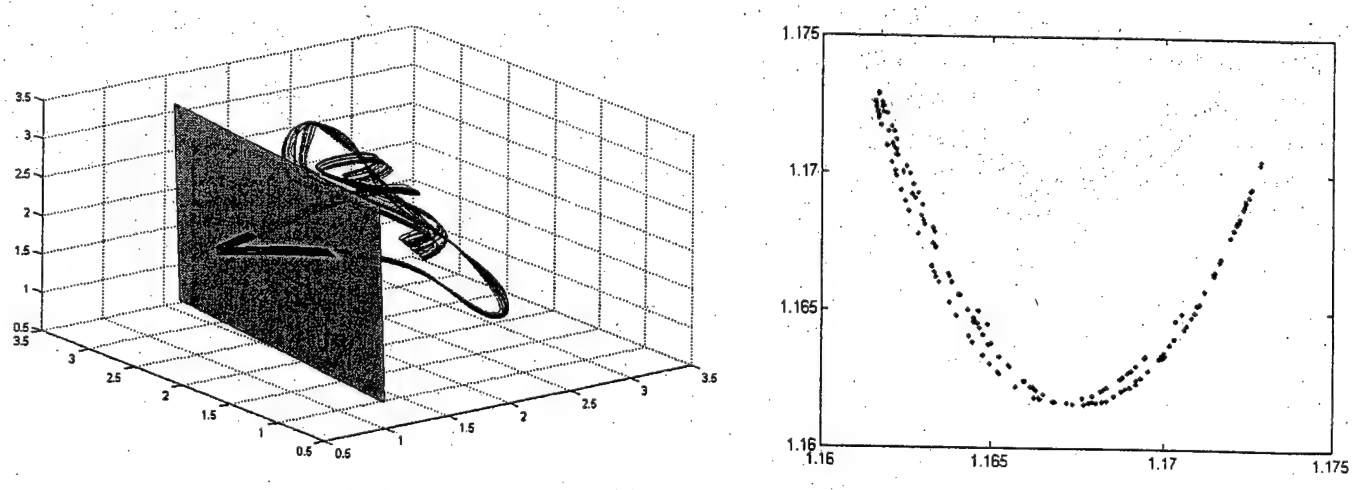

(c) ε=0.443

Fig. 31. Reconstructed phase portrait, Poincare section (left) and quasi-one-dimensional map for different ε

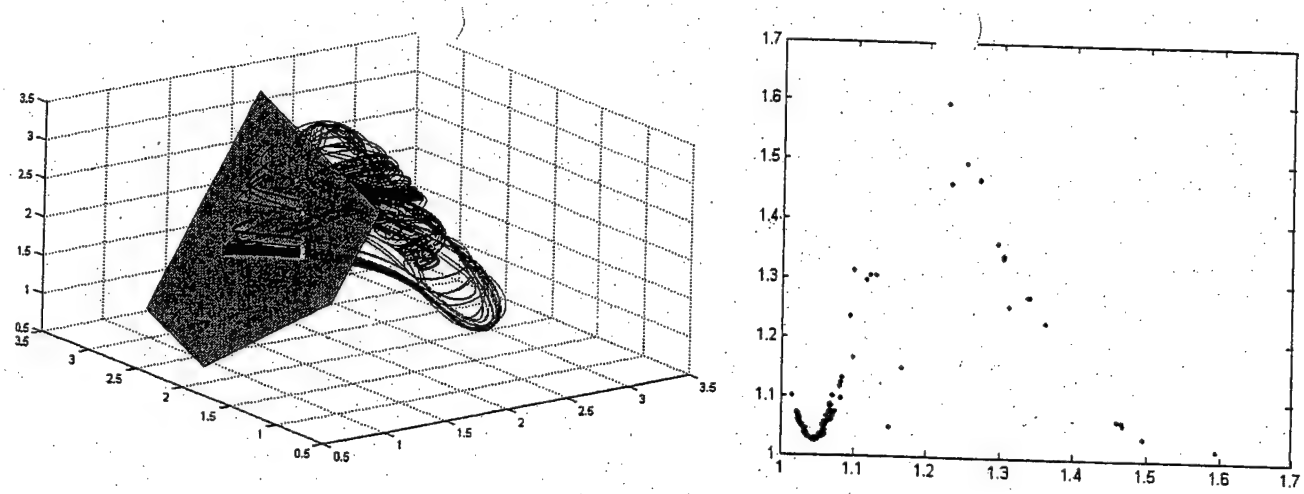

(d) ε=0.4415

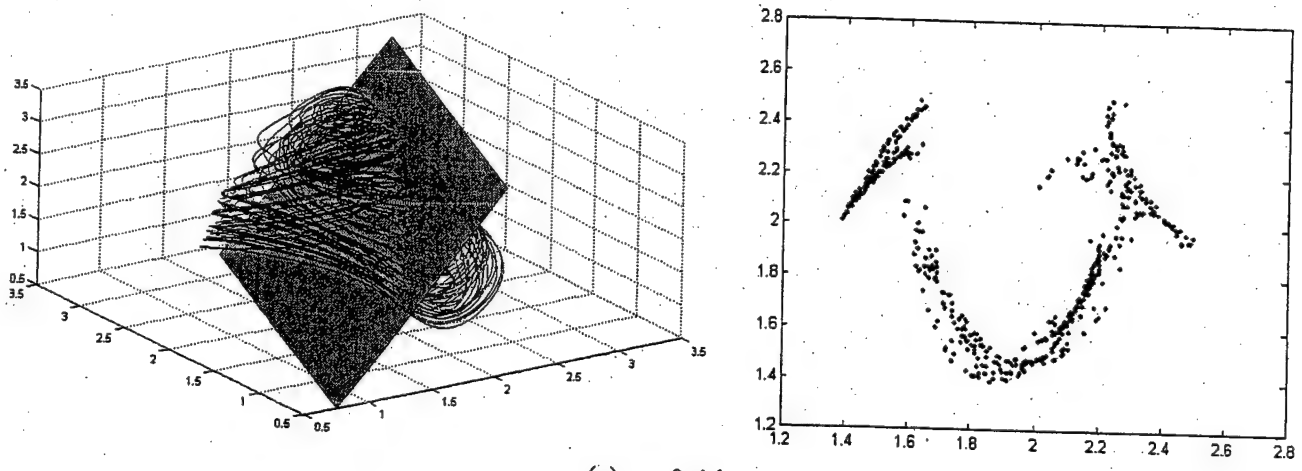

(e) ε=0.44

Fig. 31 (the end).

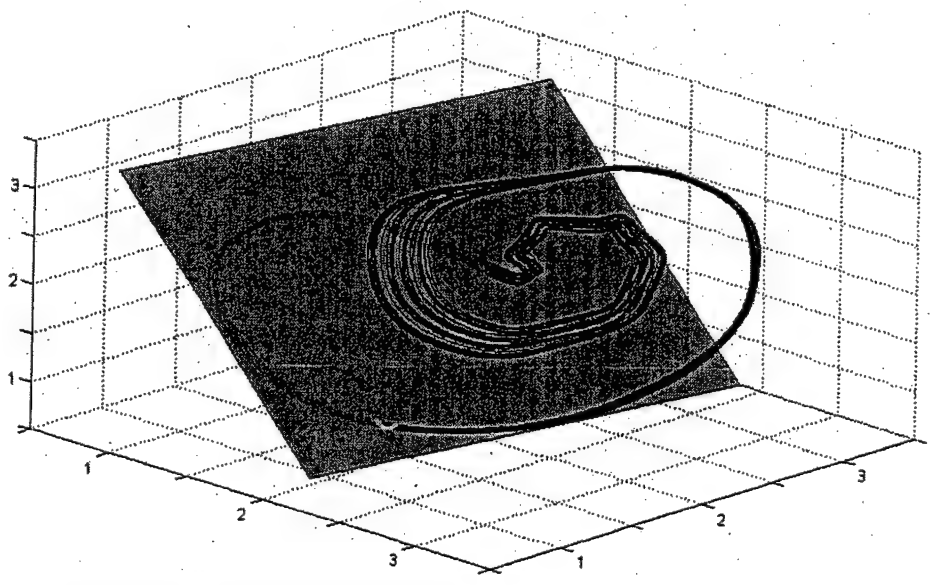

Fig. 32. Trajectory in reconstructed phase space and Poincare section for ε = 0.443

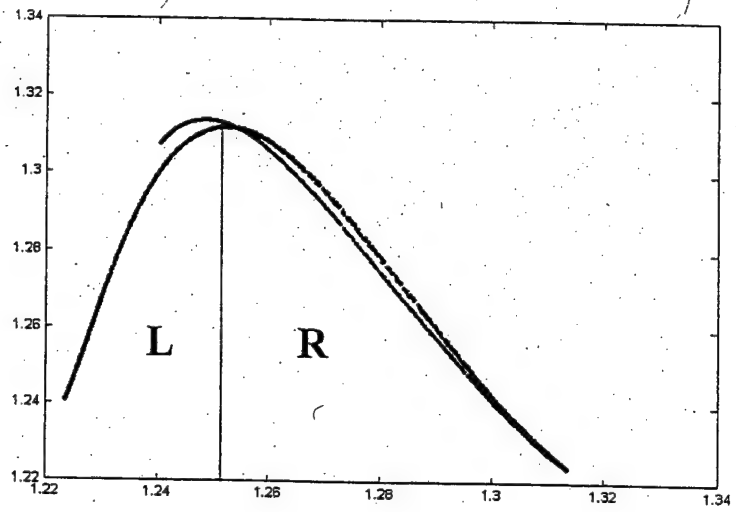

Fig.33. Map $x_{i+1}(x_i)$ for cross-section in Fig. 32.

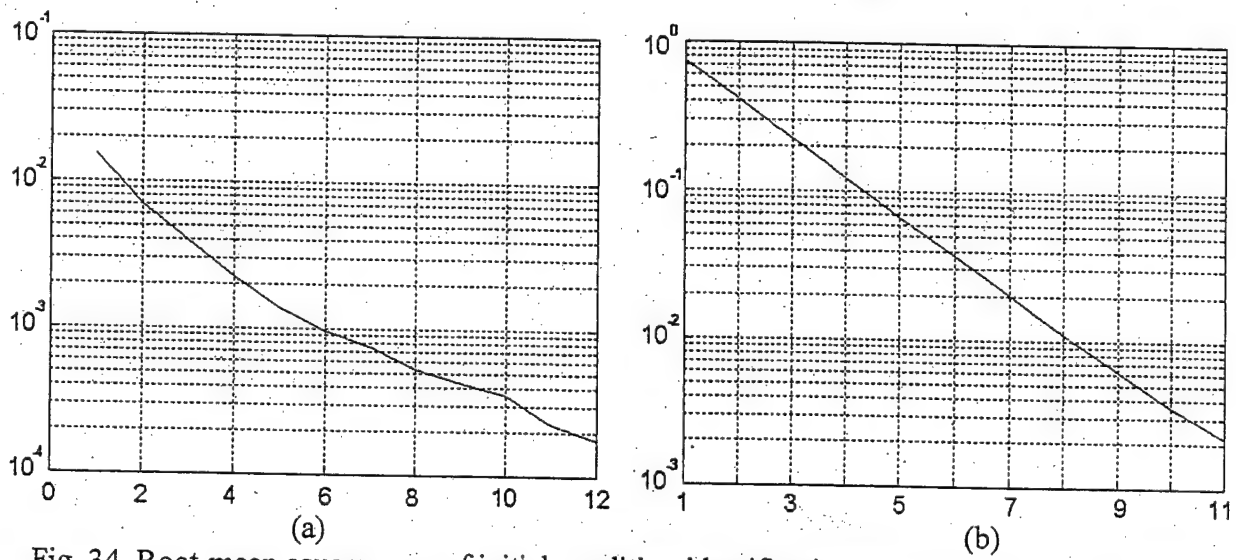

Fig. 34. Root-mean square error of initial condition identification as a function of the number of coinciding members of binary sequences belonging to different trajectories (a) for system (8) and (b) for system (15).

Therefore, if we show that with an increase of the number of coinciding members of constructed binary sequences the chaotic trajectories become closer to each other, we would get an argument (but not the proof) supporting the viewpoint of close connection between the constructed binary sequence and initial chaotic trajectory.

At Fig. 34a, horizontal axis contains the number of coinciding members of binary sequence, vertical axis – discrepancy in initial value averaged for many trajectories. Here the trajectories are considered with the specified number of coinciding members.

As one can see from Fig. 34a, the more members of binary sequences coincide, the more accurately initial points of the trajectories match.

If the introduced partition enerating then the plot above should a straight line. This is because every known sample of symbolic sequence adds in average the same amount of information about initial conditions.

For instance, Fig. 34b shows similar curve for Rossler system, for which the sequence constructed in section 5 is a symbolic one.

As one can see, the curve is practically perfect straight line. In case of TWT-system the curve has gradually decreasing slope.

Most likely this is because the used partition is only approximately generating. Nevertheless the difference between considered partition and more accurate partition, which exactly correspond to the chaotic attractor structure, could become apparent only when a rather accurate reconstruction of a signal from binary symbolic sequence is required.

The second method

As an alternative we have considered an approach to construction of symbolic dynamics based on a completely different principle. The basis of this approach to investigation of dynamics of active oscillator with delayed feedback is laid in [30], and used there for studying periodic modes.

The essence of the method is as follows. Denote by t_i the moments when the trajectory of the system moves through some value $x = x_0$. Length of time interval between succession crossings we denote as $\tau_i = t_{i+1} - t_i$.

Let us draw the plot of the map $\tau_{i+1}(\tau_i)$. Fig. 35 shows the obtained quasi-one-dimensional map for the case $x_0 = 3$. As can be seen, despite the fact that algorithm is essentially different from that described in the beginning, quasi-one-dimensional maps are almost the same.

The second method of construction of binary symbolic description is preferable compared to the first one. First, the algorithm is much more simple. Second, the constructed sequence can be more stable to noise.

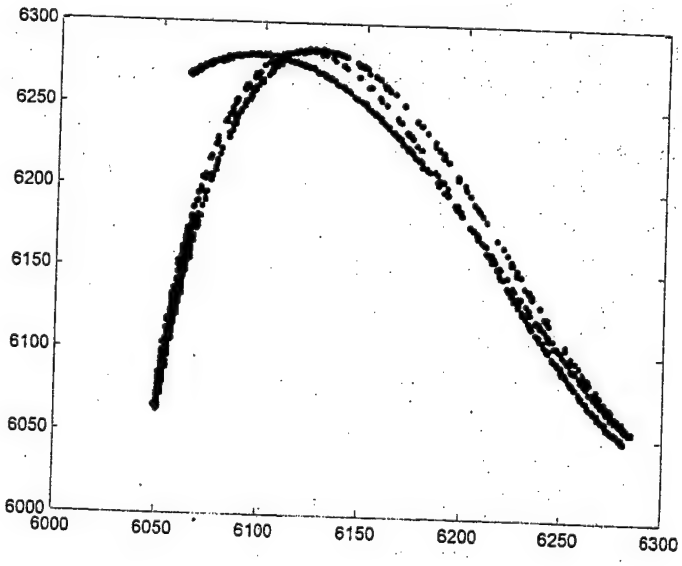

Fig. 35. Quasi-one-dimensional map $\tau_{i+1}(\tau_i)$ constructed from one-dimensional realization

To conclude, we consider) issue of permitted and prohibited s ences for both cases. Figs. 36 and 37 show histograms for different lengths of binary sequences for the first (left) and the second (right) algorithms. Binary sequences of length four are represented in decimal form on horizontal axis (Fig. 37).

As one can see, despite that methods of construction of binary sequences are completely different, catalogue of permitted sequences and relative frequencies are similar in many respects. There are no prohibited sequences among sequences of length two. Among sequences of length four the following sequences are prohibited: $LLLL$, $LLLR$, $RLLL$.

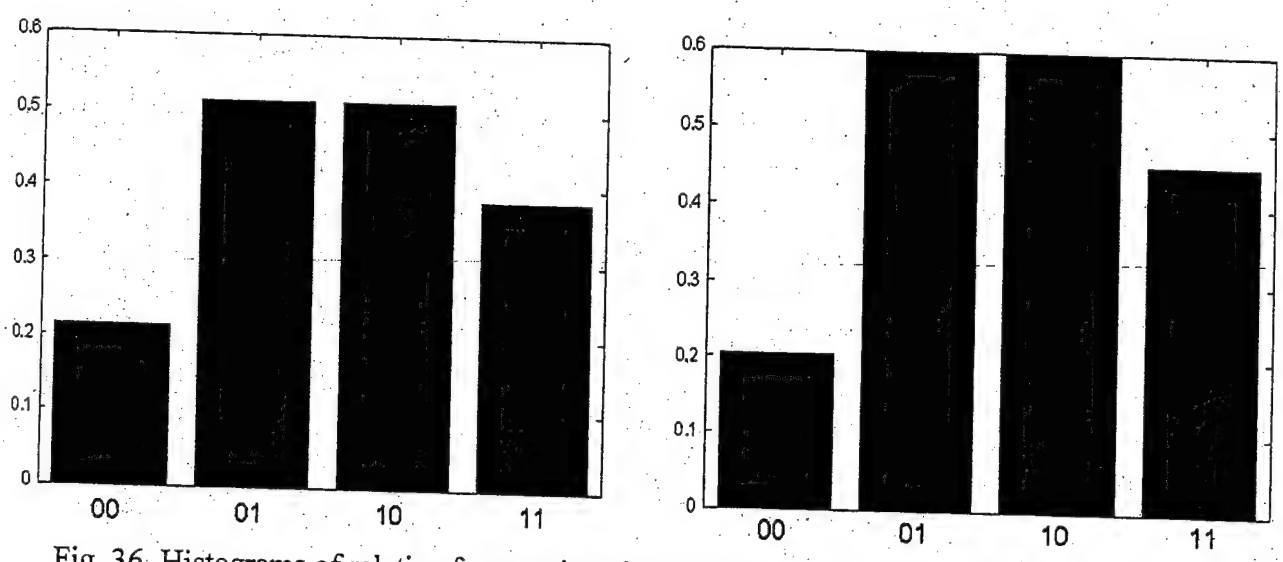

Fig. 36. Histograms of relative frequencies of permitted sequences of length 2 for two different methods of construction of binary sequence of the system (8).

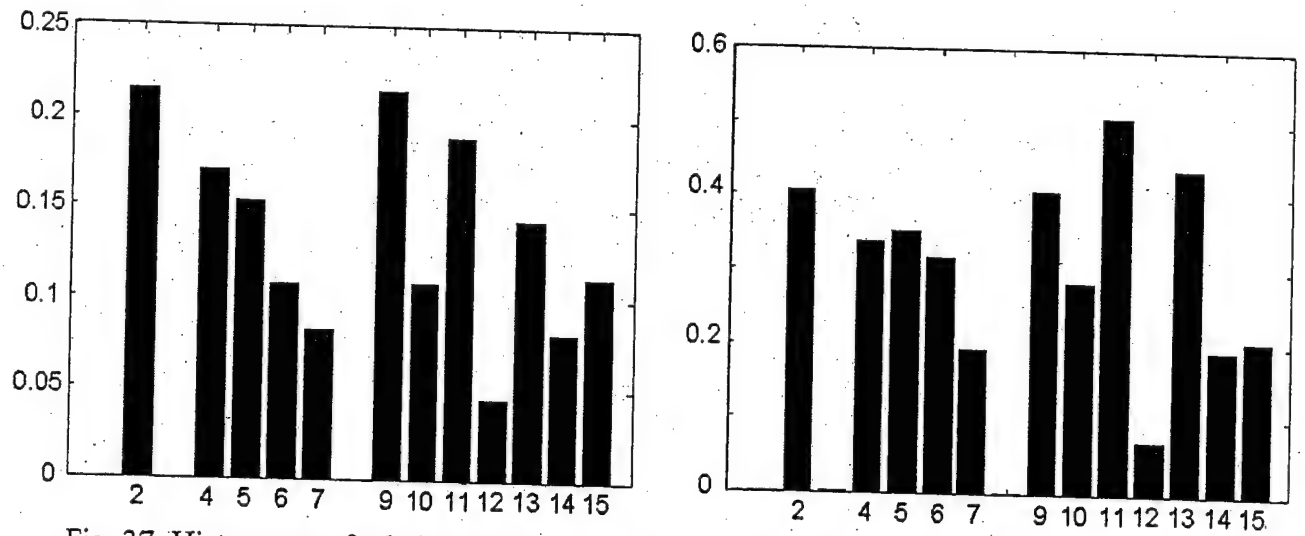

Fig. 37. Histograms of relative frequencies of permitted sequences of length 4 for two different methods of construction of binary sequence of the system (8).

6. CONCLUSIONS

The conducted investigation consists of three major stages.

The objective of the first stage of the project was a search, analysis and selection of RF devices that had potential to generate chaotic oscillations. Among potential candidates TWT, klystron, MMIC and other standard RF sources were suggested. First of all, we were interested in devices that already had mathematical models demonstrating chaotic behavior. Preference had to be given to those sources, that in a numerical simulation exhibited wide-band spectrum and low-dimensional chaos that can give a chance to construct symbolic dynamics.

The search and analysis of RF generators and their models has shown that suggested hitherto and most studied are models of devices of "electron beam – electromagnetic wave" type that demonstrate complex oscillating modes, including chaos. The most covered in the literature and most fully investigated are the models of

- two-cavity klystron
- generator based on TWT
- microtriode generator
- Pierce diode generator
- backward-wave tube generator

Note, that all these models are approximate, however they may be useful in design of the devices and can ensure qualitative understanding of their complex dynamics.

For further investigation the models of TWT generator and microtriode generator were chosen. First, because of their relatively low computational complexity compared to other models, given by partial differential equations. Second, these models can be considered generic for qualitative understanding of the processes.

Models of generators based on TWT and microtriode were investigated to find out if chaotic modes were possible. The range of parameters was localized where low-dimensional chaos exists. The estimates of attractor dimensions by of Karhunen-Loeve method and method of correlation integral were obtained.

It is shown that symbolic description of chaotic trajectories for the model of microtriode generator can be constructed via one-dimensional map. This approach is conditioned by the properties of the system and the chaotic attractor: generator based on microtriode has natural three-dimensional phase space that unambiguously sets upper bound on the dimension of chaotic attractor.

It is also shown that the knowledge of the symbolic description of the trajectory and the equations of the model allows reconstruction of the chaotic trajectory with precision limited only by precision of numerical computation.

A series of investigations was conducted to construct symbolic description for the model of TWT generator. It ascertained that symbolic description can be introduced only for relatively narrow range of parameters corresponding to low-dimensional modes at the edge of periodicity. As the driving parameter is decreased, introduction of symbolic description becomes more complicated – either a more sophisticated parameterization of the Poincare map or an

additional reversible map to eliminate ambivalence of the quasi-one-dimensional map is required. Note that the attractor does not have a simple structure that uniquely identifies the choice of the succession map. Correlation dimension of the chaotic attractor for which the introduction of symbolic dimension is possible does not exceed 2.1. There is no success in construction of symbolic description with the aid of quasi-one-dimensional map for higher-dimensional modes.

The results obtained state that symbolic description in the investigated systems allows (with some limitations) identification of chaotic modes (for example, different modes of the same generator). This is done by means of analysis of permitted and prohibited sequences of a given length. Additionally, uniqueness of the set of permitted and prohibited sequences can be used in various applications such as information transmission based on chaotic synchronization and location detection.

REFERENCES

1. Dmitriev B., Zharkov Yu., Ryskin N., Shigaev A., Chaotic operation of a delayed-feedback Klystron oscillator: theory and experiment // J. Comm. Technology and Electronics, 2001, V. 46, No. 5, p. 561.
2. Ryskin N. M., Shigaev A. M., Complex dynamics of a simple distributed self-oscillatory model system with delay // J. Technical Physics, 2002, V. 47, No. 7, p. 795.
3. Kislov V., Zalogin N., Myasin E., About nonlinear stochastic oscillations in the electron-wave generator with delayed feedback // Radio engineering & electronic physics, 1980, V. 25, No. 10, p. 2160.
4. Katz V., Appearing of chaos and its evolution in distributed generator with delay (experiment) // Izvestiya vuzov. Radiophysics, 1985, V. 28, No. 2, p. 161.
5. Kislov V., Zalogin N., Myasin E., Study of stochastic self-oscillatory processes in self-excited oscillators with delay // Radio engineering & electronic physics, 1979, V. 4, No. 6, p. 92.
6. Solntsev V., Andreevskaya T., Conditions for amplitude self-modulation in self-excited oscillator with delay // Radio engineering & electronic physics, 1983, V. 28, No. 3, p. 126.
7. Dmitrieva T.V., Ryskin N.M., Shigaev A.M., Complex Dynamics of Simple Models of Distrubyted Self-Oscilationg Delayed Feedback Systems// Nonlinear Phenomena in Complex Systems, 2001, V. 4, No 4, p. 376.
8. Afinogentov V., Chaotic oscillation in the electron beam with virtual cathode // Izvestiya vuzov. Applied Nonlinear Dynamics, 1994, V. 2, No. 5, p. 69.
9. Ponomarenko V., Trubetskov D., Complex dynamics of vacuum microtriode oscillator: numerical experiment and analogue experiment on the radiotechnical model // Izvestiya vuzov. Applied Nonlinear Dynamics, 1994, V. 2, No. 6. p. 56.
10. Dmitriev A., Kislov V., Chaotic oscillations in radiophysics and electronics. Moscow, Nauka, 1989.
11. Letellier C., Dutertre P., and Maheu B., "Unstable periodic orbits and template of the Rossler system: Toward a systematic topological characterization// Chaos , 1995, V.5, No 1, p.271.
12. Gilmor R., Topological analysis of chaotic dynamical systems// Rev. Mod. Physics, 1998, Vol. 70, N 4, p.1455.
13. Packard N.H., Crutchfield J.P., Farmer J.D., Shaw R.S. Geometry from a time series // Phys. Rev Lett., 1980, V. 45, p. 712.
14. Takens F. Detecting Strange attractors in turbulence // Dynamical Systems and Turbulence / Eds. D. Rand and L.S. Young. Lect. Notes in Math. 1980, V. 898, p. 366.
15. Rosenstein M.T. Collins J.J., De Luca C.J. Reconstruction expansion as a geometry-based framework for choosing proper delay time // Physica D, 1994, V. 73, p. 82.

16. Caputo J.G., Malrai.)B., Atten P. // Dimensions and Entrc s in Chaotic Systems Quantification of Complex Behaviour. Heidelberg, 1986. P. 180

17. Broomhead D.S., King G.P. // Physica. D, 1986, V.20, p. 217.

18. Fukanaga K. Introduction to statistical pattern recognition, Academic Press,. New York, 1972.

19. Landa P., Rosenblum M., About one method of experimental estimation of embedding dimension.// J. Techn. Phys, 1989, V.59. №1, p. 13.

20. Landa P., Rosenblum M., Comparison of methods for phase space reconstruction and attractor dimension measurement //J. Techn. Phys., 1989, V.59. №11, p. 1.

21. Grassberger P. Procaccia I. Characterization of strange attractors // Phys. Rev. Lett. 1983, V 50, No 5 p 346.

22. Farmer J.D., Ott E., Yorke J.A. The dimension of chaotic attractors// Physica D. – 1983, V.7, No 1-3. p. 153.

23. Kantz H., A robust method to estimate the maximal Lyapunov exponent of a time series// Phys. Lett. A, 1994, Vol 77, p. 185.

24. Sano M. and Sawada Y., Measurement of the Lyapunov spectrum from a chaotic time series// Phys. Rev. Lett., 1985, V 55, p. 1082.

25. Badii R., Brun E., Finardi M., Progress in the analysis of experimental chaos through periodic orbits// Rev. Modern Physics, 1994, V. 66, No. 4, p 1389.

26. Jérôme Plumecoq, Marc Lefranc, From template analysis to generating partitions I: Periodics orbits, knots and symbolic encodings// Physica D, 2000, V.144, p. 231.

27. Jérôme Plumecoq, Marc Lefranc, From template analysis to generating partitions II: Characterization of the symbolic encodings// Physica D, 2000, V. 144, p. 259.

28. Hao bai-Lin, Elementary Symbolic Dynamics and Chaos in Dissipative Systems// World Scientific, Singapore, 1989.

29. Dmitriev A.S., Kassian G., and Khilinsky A., Chaotic synchronization. Information viewpoint// Int. J. Bifurcation and Chaos, 2000, V. 10, No. 4, p. 749.

30. Dmitriev A.S., Kaschenko S.A., Dynamics of autogenerator with delayed feedback // J. Comm. Technology and Electronics, 1989, V. 34, No 12. p. 16